Boundary layer versus free tropospheric CO budget and variability over the United States during summertime

A. Boynard,[1] Gabriele G. Pfister,[1] and David P. Edwards[1]

Received 16 June 2011; revised 21 December 2011; accepted 27 December 2011; published 23 February 2012.

[1] The regional Weather Research and Forecasting Model with Chemistry (WRF-Chem) version 3.2 is used to analyze the carbon monoxide (CO) budget and spatiotemporal variability over the United States in summer 2008. CO tracers for different emission sources are used to separate the modeled CO fields into the contributions from individual sources (pollution inflow to the model domain, chemical production within the model domain, and local emissions by type). The implementation of tagged CO tracers into WRF-Chem constitutes an innovative aspect of this work. We evaluate WRF-Chem CO concentrations using aircraft, satellite, and surface observations. The model reproduces fairly well the observed CO concentrations for the entire altitude range but tends to underestimate fire emissions and overestimate anthropogenic sources and CO from pollution inflow. Evaluation results also show that the model gives a good representation of background CO mixing ratios with mean biases better than ~15 ppbv in the free troposphere (FT) and less than 20 ppbv toward the surface. The analysis of the CO budget over the contiguous United States shows that at the surface, CO from inflow is the dominant source, with a mean relative contribution of 63 ± 19%. Anthropogenic and photochemically produced CO contribute to surface CO to a lesser extent (18 ± 14% and 14 ± 8%, respectively). The average contribution from fire emissions to surface CO during the period examined is small (2 ± 5%) but can have a large impact in certain regions and times. Similar trends are found in the planetary boundary layer (PBL). In the FT, the average CO relative contributions are estimated as 84 ± 12% for CO from inflow, 5 ± 4% for anthropogenic CO, 9 ± 7% for photochemically produced CO, and 1 ± 5% for CO from fires. Using WRF-Chem simulations, we also examine the representation of surface and PBL CO concentration variability that would be captured by current near infrared (NIR) and thermal infrared (TIR) satellite observations. We find that CO total columns are impacted by variability in the lowermost troposphere (LMT) at the ~10% level, indicating limited sensitivity for air quality applications. The same is generally true for the FT CO column obtained from TIR measurements, although this does provide a good measure for capturing the pollution inflow variability and is therefore valuable in providing initial and boundary conditions to constrain regional models. We further analyze the situations under which the LMT concentrations obtained from recently demonstrated multispectral (NIR + TIR) observations capture the surface CO variability.

Citation: Boynard, A., G. G. Pfister, and D. P. Edwards (2012), Boundary layer versus free tropospheric CO budget and variability over the United States during summertime, *J. Geophys. Res.*, *117*, D04306, doi:10.1029/2011JD016416.

1. Introduction

[2] Carbon monoxide (CO) plays an important role in governing tropospheric chemistry. The main sources of CO are fossil fuel and biomass combustion, and oxidation of methane and nonmethane hydrocarbons [e.g., *Duncan and Logan*, 2008; *Holloway et al.*, 2000]. The major sink of CO is the reaction with the hydroxyl radical (OH), the principal oxidant of the troposphere [e.g., *Crutzen and Zimmermann*, 1991]. Depending on concentrations of nitrogen oxides (NO_x), reactions involving CO can be a source or a sink for ozone [e.g., *Crutzen*, 1973; *Logan et al.*, 1981]. In addition, reactions of CO with other trace gases may have a significant impact on climate change by affecting methane and tropospheric ozone chemistry [e.g., *Daniel and Solomon*, 1998; *Thompson and Cicerone*, 1986; *Wigley et al.*, 2002]. With a mean lifetime of 2 months in the troposphere [*Seinfeld and*

[1]Atmospheric Chemistry Division, National Center for Atmospheric Research, Boulder, Colorado, USA.

0148-0227/12/2011JD016416

Table 1. WRF-Chem Configuration Used in This Study

Atmospheric Processes	WRF-Chem Configuration[a]
Radiation	LW: RRTM [*Mlawer et al.*, 1997]; SW: Goddard [*Chou and Suarez*, 1994]
Surface layer	Monin-Obukhov (Janjic Eta) scheme
Land surface model	RUC land-surface model [*Smirnova et al.*, 1997, 2000]
Planetary boundary layer	MYJ scheme [*Mellor and Yamada*, 1982; *Janjic*, 1996, 2002]
Cumulus	Grell-Devenyi ensemble scheme
Microphysics	Thompson graupel scheme
Gas-phase chemistry	MOZART
Aerosol chemistry	GOCART
Photolysis	Madronich F-TUV [*Madronich*, 1987]

[a]MOZART, Model for Ozone and Related Chemical Tracers; GOCART, Goddard Chemistry Aerosol Radiation and Transport; LW: RRTM, Long Wave: Rapid Radiative Transfer Model; SW: Goddard, Short Wave: Goddard; RUC, Rapid Update Cycle; MYJ, Mellor-Yamada, Janic; F-TUV, Fastr Tropospheric Ultraviolet Visible.

Pandis, 2006], CO is used as a tracer of long-range transport of pollution [e.g., *Badr and Probert*, 1994; *Edwards et al.*, 2006; *Jacob et al.*, 2003; *Jaffe et al.*, 2004]. Furthermore, as a dominant sink for OH [*Logan et al.*, 1981] and a precursor for tropospheric ozone, CO also has an impact on air quality (AQ). Toxic to humans and the environment at very high concentrations, it is characterized as a "criteria pollutant" by the *U. S. Environmental Protection Agency* [1991, 2000]. For these reasons, it is important to understand better the sources contributing to the CO budget and its variability in the troposphere, particularly at the surface and in the planetary boundary layer (PBL). This has been studied in several papers by applying CO tracers incorporated into global chemistry transport models [e.g., *Bey et al.*, 2001; *Granier et al.*, 1999; *Peng et al.*, 2007; *Pfister et al.*, 2004, 2010], but to our knowledge there have been few studies applying this technique using a regional model [*Huang et al.*, 2010; *Pfister et al.*, 2011b].

[3] Over the United States, several studies on CO have already been reported, with different purposes such as satellite validation [*Emmons et al.*, 2007], pollution transport analysis [*McMillan et al.*, 2008; *Pfister et al.*, 2010; *Zhang et al.*, 2008], CO and ozone relationship [*Chin et al.*, 1994], or satellite Observation System Simulation Experiment (OSSE) analyses [*Edwards et al.*, 2009]. Other studies have been performed on a more localized scale [e.g., *Hudman et al.*, 2008; *Lamarque et al.*, 2003; *McMillan et al.*, 2010; *Miller et al.*, 2008]. However, the lack of sufficiently sensitive in situ observations at the surface and in the lowermost troposphere (LMT) on the scale of the United States makes difficult the study of CO for AQ purposes.

[4] Satellites constitute a unique platform for observing the atmosphere and have been extensively used to better understand tropospheric composition and dynamics [e.g., *Edwards et al.*, 2006; *Kopacz et al.*, 2010; *Turquety et al.*, 2008]. The remote sensing of the LMT is challenging, and despite providing good long-term spatial coverage with some vertical profile information, the question arises to what extent these observations can be used for estimating surface concentrations for AQ applications. Currently, CO retrievals are based on (1) near infrared (NIR) radiances at 2.3 μm mainly sensitive to the total column [e.g., *Deeter et al.*, 2009], (2) thermal infrared (TIR) radiances at 4.6 μm primarily sensitive to the free troposphere (FT) [e.g., *Deeter et al.*, 2004], and (3) multispectral (NIR + TIR) radiances that may provide sensitivity to the LMT column [*Deeter et al.*, 2011; *Worden et al.*, 2010]. This work is undertaken in the framework of the preparation for the future NASA Geostationary Coastal and Air Pollution Events (GEO-CAPE) mission with launch toward the end of the decade (J. Fishman et al., Progress report on NASA's GEO-CAPE mission, submitted to *Bulletin of the American Meteorological Society*, 2012). One of the major objectives of GEO-CAPE is to improve the ability to observe and understand AQ on continental scales and to help define policies for pollution control.

[5] In this work, we first present an analysis of the CO budget and variability during the summertime of 2008 over the contiguous United States using the regional Weather Research and Forecasting Model with Chemistry (WRF-Chem V3.2). In the second part of this work, WRF-Chem is used to analyze how useful the current satellite CO measurements are for capturing the variability of surface concentration. The structure of the paper is as follows. In section 2, the WRF-Chem model and simulations are described. We evaluate the model by comparing modeled CO concentrations to aircraft measurements, satellite retrievals and ground-based observations in section 3. An analysis of the CO spatial distribution and budget over the contiguous United States is given in section 4, while we analyze the CO vertical distribution in section 5. The use of satellite CO observations for AQ monitoring is discussed in section 6, and conclusions are given in section 7.

2. Model Simulations

[6] For this study, simulations are performed with the regional chemistry transport model WRF-Chem, version 3.2. WRF-Chem is the Weather Research and Forecasting (WRF) model [*Skamarock et al.*, 2008] coupled with Chemistry [*Grell et al.*, 2005]. The model simulates the emission, transport, mixing, and chemical transformation of trace gases and aerosols simultaneously with the meteorology. The version of the model used here includes online computation of dynamical inputs (winds, temperature, boundary layer, clouds, rain etc.), transport (advective, convective, and diffusive), dry deposition [*Wesely*, 1989], gas phase chemistry, radiation and photolysis rates, and biogenic emissions. The model also included anthropogenic and fire emissions that are calculated off-line. The model configuration is detailed in Table 1.

[7] The WRF-Chem gas-phase chemical mechanism is that from Model for Ozone and Related Chemical Tracers, version 4 (MOZART-4) [*Emmons et al.*, 2010], which includes 85 gas-phase species, 39 photolysis and 157 gas-phase reactions, and is coupled to the aerosol scheme Goddard Chemistry Aerosol Radiation and Transport (GOCART) model [*Chin et al.*, 2002]. The horizontal resolution is set to 24 km $\times$ 24 km, and we use 51 vertical levels from the surface up to 10 hPa. The meteorological initial and boundary conditions are based on the National Centers for Environmental Prediction (NCEP) Global Forecast System (GFS) analyses provided every 6 h with 1-degree horizontal resolution and 27 vertical levels from the surface up to 10 hPa. More information on the meteorological data can be

found at http://dss.ucar.edu/datasets/ds083.2. The chemical initial and boundary conditions, spatially and temporally varying (6 h), are constrained by global chemical transport simulations from MOZART-4 with 0.7° × 0.7° horizontal resolution [*Pfister et al.*, 2011a]. In addition to the chemically active species, four CO tracers are incorporated in the WRF-Chem simulation [*Pfister et al.*, 2011b]: CO emitted from regional anthropogenic (CO-ANTHRO) and fire (CO-FIRE) sources, CO produced photochemically within the domain (CO-CHEM) and CO pollution inflow (CO-BC). The latter tracks the transport of CO at the lateral boundaries through the domain. CO-CHEM is related to production from hydrocarbons emitted within the domain as well as hydrocarbons entering the domain at the lateral boundaries. These four sources are assumed to represent the major sources of the modeled total CO. Direct biogenic emissions of CO are not accounted for, but these represent a very small part of the total surface concentration. Using these tracers allows examination of the different components contributing to observed CO concentrations.

[8] The anthropogenic emissions used within the WRF-Chem model are obtained from the EPA 2005 U.S. National Emissions Inventory (NEI-2005). These emissions are provided separately for weekday, Saturday and Sunday with hourly resolution on a 4 km × 4 km grid. Biomass burning emissions are obtained from the Fire Inventory from NCAR (FINN V1) [*Wiedinmyer et al.*, 2006, 2010] and are distributed in the model vertically following the online plume-rise module [*Freitas et al.*, 2007]. Biogenic emissions are calculated online from the Model of Emissions of Gases and Aerosols from Nature (MEGAN) [*Guenther et al.*, 2006]. The CO anthropogenic emissions totaled over the contiguous United States for the time period 10 June to 10 July 2008 are estimated as 5.7 Tg C while the CO fire emissions are estimated at 0.4 Tg C.

[9] The WRF-Chem simulation starts on 10 June 00 UT and output is written every 2 h. After one week, the sum of CO tracers (CO-ANTHRO + CO-FIRE + CO-CHEM + CO-BC), which are set to cover all the major CO sources [*Pfister et al.*, 2011b], is within 10% of the total CO at the surface. After 13 days, the tracers are well spun up and the difference between the tracer sum and the total CO is less than 3%. The small discrepancy is accounted for by biogenic CO emissions and numerical inaccuracy. To avoid effects due to spin-up, we limit all analysis that involves CO tracers to the time period from 24 June to 10 July 2008.

3. Model Evaluation

[10] The model is evaluated by comparing CO concentrations to different data sets representing different observational scales: aircraft, satellite and surface observations. First, the model is compared to aircraft measurements obtained from the Stratosphere-Troposphere Analyses of Regional Transport (START08) field campaign [*Pan et al.*, 2010] that took place over the central North America in spring and summer 2008. In addition, we make use of measurements taken as part of the European-funded Measurements of ozone, water vapor, carbon monoxide and nitrogen oxides by Airbus in-service aircraft (MOZAIC) program [*Marenco et al.*, 1998]. The model is then evaluated with the CO total column version 4 product retrieved from the Measurement of Pollution in the Troposphere (MOPITT) instrument onboard the NASA EOS/Terra satellite [*Deeter et al.*, 2010]. Finally we compare model results with surface measurements provided by two networks: EPA Air Quality System (EPA U.S. air quality system data mart, 2008, available at http://www.epa.gov/ttn/airs/airsaqs/detaildata/downloadaqsdata.htm) and the Southeastern Aerosol Research and Characterization Study experiment (SEARCH) network (available at http://www.atmospheric-research.com/public/index.html) [*Hansen et al.*, 2003].

[11] During the simulation time period, aircraft observations from the Arctic Research of the Composition of the Troposphere from Aircraft and Satellites (ARCTAS) field campaign [*Jacob et al.*, 2010] were also available. A detailed evaluation of the model over California with ARCTAS observations is given by *Pfister et al.* [2011b].

3.1. Comparisons to Aircraft Data

3.1.1. Comparisons to START08 Observations

[12] The START08 field experiment was designed to study key transport processes impacting the chemical-microphysical distribution of the extratropical upper troposphere and lower stratosphere and to investigate the behavior of the extratropical tropopause. Six scientific flights were conducted with the NFS/NCAR Gulfstream-V (GV) aircraft in June 2008 covering the generally clean region over the mid United States. The measurements of CO are derived from the NCAR/NSF C-130 CO vacuum UV resonance fluorescence instrument [*Gerbig et al.*, 1999] with an uncertainty of ± (2 ppbv +5%) [*Vogel et al.*, 2011].

[13] For the evaluation of the modeled CO fields, we use 1 min merged data, interpolate the modeled CO fields to the time and location of the aircraft measurements and average the observed and modeled CO mixing ratios over 1 km height intervals. Figure 1 shows comparisons of average modeled and observed CO vertical profiles for the GV for all collocated data. CO tracer vertical profiles are depicted in order to support the analysis. For the entire altitude range, observed CO mixing ratios vary between 100 and 150 ppbv, and the variability in observed CO is about 20 ppbv. Overall, the model captures the vertical gradient in CO mixing ratios and the magnitude well and slightly overestimates the CO mixing ratios with mean biases of about 15 ppbv. In the FT, where CO from inflow is dominant (see CO-BC profile), the lowest biases are found and the model underestimates the variability range. Toward the surface, where local emissions increase (see CO-ANTHRO profile), the absolute mean biases are higher and the model tends to slightly overestimate the variability in CO. The comparison of the model to START08 data shows that the model gives a fairly good representation of background CO mixing ratios.

3.1.2. Comparison to MOZAIC Observations

[14] MOZAIC has made regular measurements of CO by autonomous instruments deployed aboard five commercial airliners since 2001 to support studies of atmospheric composition change under the influence of human activity. CO measurements are based on an infrared analyzer with an accuracy of ± (5 ppbv + 5%) for a 30 s response time [*Nedelec et al.*, 2003]. During the entire simulation period, there were 37 flights over the United States including 9 over Philadelphia, 7 over Atlanta, 13 over Dallas, and 8 over Portland. This additional observation set complements

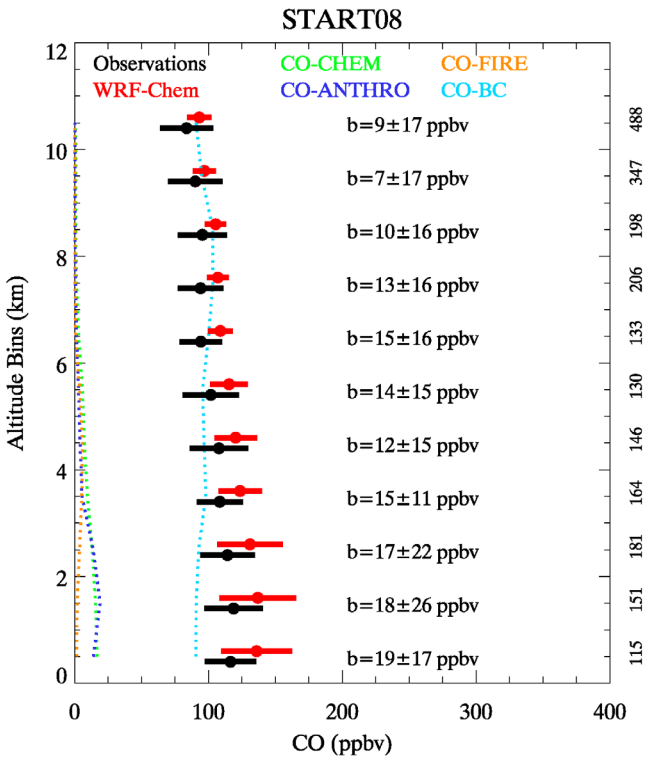

Figure 1. Mean (dots) and standard deviation (bars) of observed (black) and modeled (red) CO vertical profiles for Gulfstream-V (GV) flights during the START08 campaign. Mean bias (*b*) and standard deviation between model and observations are given for each altitude bin in each plot. Vertical profiles of CO tracers are also displayed (dotted lines). The number of observations is specified on the right vertical axis.

START08 measurements, as MOZAIC provides data representative of mostly polluted regions.

[15] Comparison to MOZAIC observations is based on the same method as that used for START08 observations. Figure 2 shows the observed and modeled CO profiles interpolated to the time and location of the aircraft for the four airports. Overall, the model results reproduce the magnitudes and mean profile behavior of observed CO mixing ratios well, but show more variability with higher mixing ratios toward the surface. Over Philadelphia, Atlanta and Dallas, the model generally gives a fairly good representation of the free tropospheric CO with mixing ratios of about 100 ppbv. Over Portland, the aircraft observations show enhanced values of CO around 5–7 km, which is also reproduced in the model, but with higher mixing ratios (biases up to 52 ppbv). This region is largely influenced by pollution inflow coming from the west, as shown by the CO-BC vertical profile, which is known to be overestimated in the model [*Pfister et al.*, 2011a]. Toward the surface, the absolute bias is higher owing to the influences of local sources (emission and transport). The bias significantly increases up to 105 ppbv over Atlanta and Philadelphia, which are strongly dominated by anthropogenic CO as shown by the CO-ANTHRO vertical profile. The variability in the observed and modeled CO generally increases near the surface, reflecting the importance of localized sources.

3.2. Comparison to MOPITT Observations

[16] In this comparison, we use the MOPITT version 4 (V4) CO total column product [*Deeter et al.*, 2010]. This uses TIR channel signals in conjunction with a maximum a posteriori (MAP) optimal estimation retrieval approach [*Deeter et al.*, 2003; *Rodgers and Connor*, 2003]. MOPITT V4 retrievals have undergone extensive validation studies covering a wide variety of locations and environments, and results show biases of less than 1% at the surface, 700 hPa and 100 hPa, and a bias of near −6% at 400 hPa [*Deeter et al.*, 2010; *Emmons et al.*, 2009]. However, the sensitivity of TIR retrievals to CO concentration in the LMT depends on the prevailing thermal contrast between the surface and near-surface atmosphere, and in general, the CO total column retrieval is most sensitive to CO in the FT.

[17] For the comparison of WRF-Chem and MOPITT CO total column, the modeled profile is first interpolated to the time and location of the retrieval. Then we apply the averaging kernel and a priori profile associated with each MOPITT measurement to the interpolated modeled profile as described by *Emmons et al.* [2009]. As daytime MOPITT retrievals have better information content than nighttime data [*Deeter et al.*, 2010], we only use daytime observations for the comparison.

[18] Figure 3 shows the spatial distribution of the MOPITT and the corresponding WRF-Chem simulated CO total column averaged over the period 10 June to 10 July 2008 and the relative differences. Note that the model is evaluated over the entire simulation period since the CO total column is not affected by the spin-up of the tracers. Both MOPITT and WRF-Chem observe similar spatial patterns with an enhancement of CO over the regions impacted by fires (U.S. West Coast) and anthropogenic emissions (U.S. East Coast). Considering the entire simulation domain, the model matches summertime MOPITT CO total column fairly well with a mean bias of 8 ± 14e16 molecules cm^{-2} (5 ± 7%) and a correlation coefficient of 0.90. Statistics are also calculated separately over the contiguous United States. Results show the model biased slightly high by 6 ± 13e16 molecules cm^{-2} (3 ± 7%) with a correlation coefficient of 0.90. Table 2 summarizes the comparison results.

[19] Some of the discrepancies observed are due to uncertainties in the model emission estimates, in particular close to source regions and also in the transport and chemistry. For example, the model underestimates CO in the region of California, which is mostly owing to an underestimate of the WRF-Chem fire emissions [*Pfister et al.*, 2011b]. We also see an overestimation at the southern part of the domain suggesting that the boundary conditions bring in too much CO. This is also the case at the western boundary, which is corroborated by *Pfister et al.* [2011a], who found a high bias in the MOZART results for the western boundaries. Uncertainties in the retrievals further add to the discrepancies. As previously mentioned, the MOPITT retrieval sensitivity depends on the thermal contrast between the surface and the overlaying layer, which is different over land and ocean. The analysis of the MOPITT averaging kernel functions (not displayed here) indicates that the comparison of MOPITT CO retrievals mainly provides an evaluation of the modeled CO in the lower and

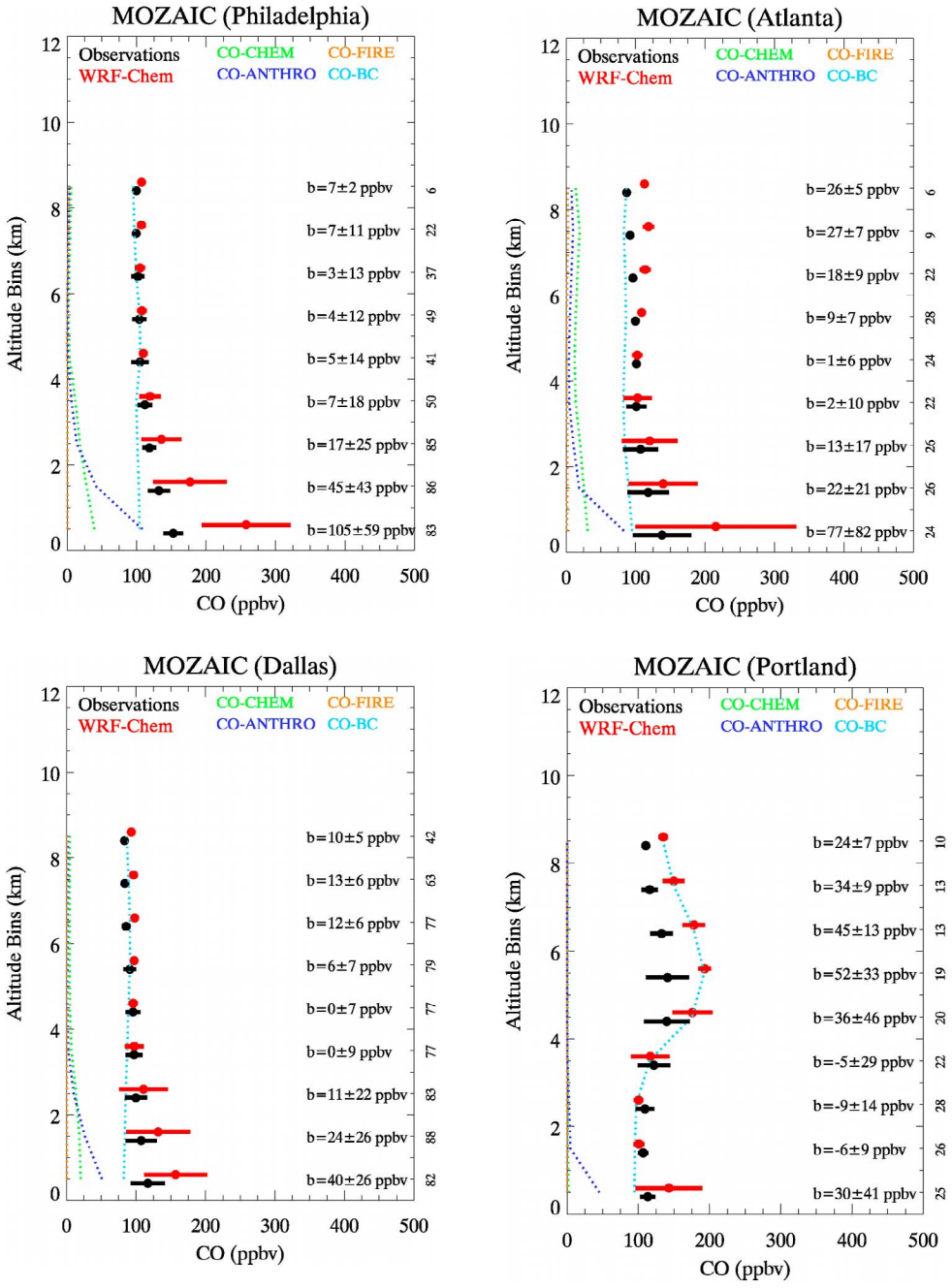

Figure 2. Same as Figure 1 but for MOZAIC flights.

middle troposphere over land, but in the upper troposphere over the ocean.

[20] The comparison to MOPITT satellite observations leads to similar conclusions from the previous evaluation with aircraft measurements: overall the model reproduced the observed CO concentrations well, but tends to overestimate the CO from pollution inflow. Moreover the results show that the model underestimates fire emissions.

3.3. Comparison to Surface Monitoring Measurements

3.3.1. Overall Comparison

[21] The EPA surface monitoring data set includes 157 urban, 132 suburban, and 31 rural sites; that is, 90% of the sites are specified as being located in either urban or suburban environments. The main source of CO in cities arises from mobile sources (according to EPA studies), and for this reason, monitoring sites are mostly located near roadways and major intersections, which are difficult to capture with the model spatial resolution. In addition, most of these measurements (80%) are of a low-resolution (multiples of 100 ppbv), which impacts the model evaluation. Although these low-resolution EPA observations have some limitations, they are still useful for evaluating the overall performance of the model at the surface. Additional CO observations extracted from the SEARCH monitoring network are also used for the evaluation of the model

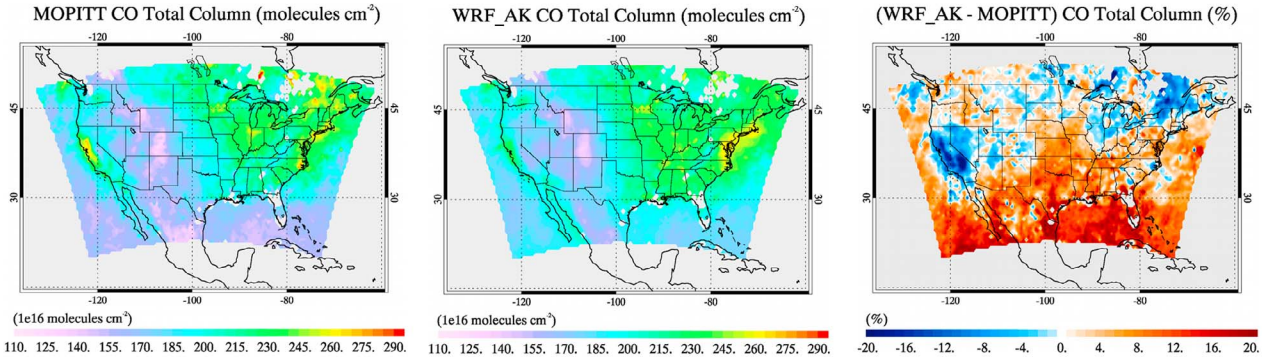

Figure 3. CO total column retrieved from MOPITT averaged over the period 10 June to 10 July 2008 and corresponding WRF-Chem simulation convolved with the MOPITT averaging kernel. The relative difference between WRF-Chem and MOPITT is also illustrated.

performance. This network is composed of eight highly instrumented stations (4 urban, 1 suburban, and 3 rural sites) in the southeast [*Hansen et al.*, 2003; *Edgerton et al.*, 2005, 2006]. This data set complements the EPA observations, owing to their high resolution and different location.

[22] For model evaluation, we interpolate the surface modeled CO mixing ratios to the time and location of the observations and produce hourly averaged observed and modeled CO mixing ratios over an 8 h moving window. This time period is used for establishing the CO National Ambient Air Quality Standards and also serves to decrease measurement noise. Figure 4 shows the time-averaged observed CO mixing ratios and biases at each of the EPA and SEARCH surface monitoring sites. We focus the spatial comparison to a time window in the afternoon when the PBL is well developed and when the model uncertainty in the PBL height tends to be smaller. The maps show that the spatial coverage of high-resolution EPA sites is very poor in the center and the west of the United States, but that low-resolution EPA sites do provide information in these regions. Note that Figures 4b and 4d include both EPA and SEARCH high-resolution measurements. Figures 4a and 4b show that low-resolution and high-resolution measurements are consistent. CO mixing ratios are generally highest on the East Coast of the United States and in parts of California, and lowest at rural sites and in the central United States. Figures 4c and 4d show that the model overestimates CO mixing ratios in areas like Southern California and the east of the United States where the time-averaged CO surface concentration is strongly dependent on anthropogenic sources, as we discuss below. Negative biases are found in Northern California, a region strongly influenced by fires during the simulation time period and also in the center of the United States, where pollution inflow is the dominant source.

[23] In order to distinguish regions influenced mainly by anthropogenic CO from those influenced by CO from fire or pollution inflow, we further analyze the evaluation results by splitting the United States into four subregions (Northern and Southern California, center and east of the United States). As low- and high-resolution measurements are generally consistent, we combine both in the following analysis. Figure 5 displays the time series of observed and modeled surface CO mixing ratios averaged over each of the U.S. subregions. The CO tracer time series are also shown, and indicate that the east of the United States and Southern California are dominated by anthropogenic CO emissions while the Center of the United States is mostly influenced by pollution inflow. Moreover CO produced chemically is greatest in the east of United States and fire emissions are a strong contribution in the west of the United States during the period considered.

[24] Northern California (Figure 5a) is characterized by CO mixing ratios of about 400 ppbv and can reach up to 750 ppbv during the period of intense fires in this region (for DOY (Day of Year) between 175 and 180). WRF-Chem reproduces the CO peaks related to the fires but underestimates the concentrations, which is mainly owing to an underestimate of fire emissions used in the model [*Pfister et al.*, 2011b]. Overall, this results in CO mixing ratios with a mean bias of -136 ± 89 ppbv. The CO tracer contributions show an increase of fire emission contribution during the intense fire period and a low contribution from anthropogenic CO. The model reproduces well the fire peaks and the correlation between WRF-Chem and observations is high (0.90). In Southern California (Figure 5b), the observed

Table 2. Performance Statistics of WRF-Chem Simulation for the CO Total Column for the Period 10 June to 10 July 2008[a]

	MOPITT CO (1×10^{16} molecules cm^{-2})	Modeled CO (1×10^{16} molecules cm^{-2})	Bias (1×10^{16} molecules cm^{-2})	Correlation Coefficient
Whole domain	193 ± 30 (191)	201 ± 25 (199)	8 ± 14 ($5 \pm 7\%$)	0.90
United States	198 ± 28 (198)	204 ± 28 (207)	6 ± 13 ($3 \pm 7\%$)	0.90

[a]Mean concentration, mean bias, associated standard deviation, and correlation coefficient for observed (MOPITT) and modeled CO are provided. Median values are in parentheses.

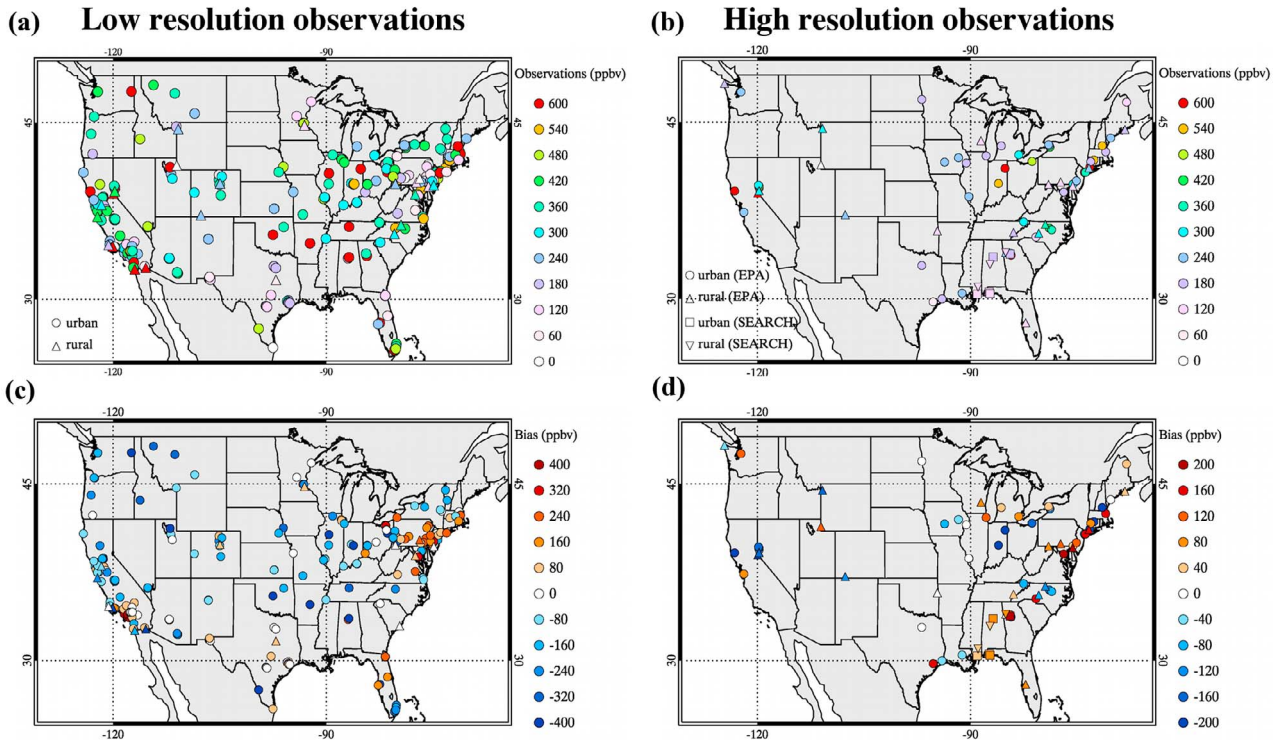

Figure 4. Spatial distributions of the time-averaged observed CO mixing ratio and bias between model and observation for (a and c) low-resolution EPA sites and for (b and d) high-resolution EPA and Southeastern Aerosol Research and Characterization Study experiment (SEARCH) sites. CO mixing ratio and bias are averaged in a time window in the afternoon between 1200 and 1800 LT.

CO mixing ratios are about 400 ppbv and WRF-Chem overestimates the CO mixing ratios with a mean bias of 95 ± 93 ppbv. This region is largely dominated by anthropogenic CO in both magnitude and variability as shown by the CO-ANTHRO time series, followed by CO from inflow (mixing ratios of about 100 ppbv). Time series of observed and modeled CO mixing ratios are characterized by discrepancies in the timing of CO peaks, which explains the noncorrelation found between WRF-Chem and observations. This could be explained by an incorrect simulation of the evolution of the PBL or an incorrect time allocation of CO emission in the emission inventory [*Pfister et al.*, 2011b]. A significant improvement of the correlation between WRF-Chem and observations is found (0.80) when CO mixing ratios are averaged on a daily basis. This indicates that the model reproduces well the CO temporal variability at synoptic scale. A more detailed analysis of the evaluation of modeled CO over California can be found in the work of *Pfister et al.* [2011b].

[25] The model also is biased high in the east of the United States (Figure 5c), but in contrast to Southern California reproduces fairly well the diurnal cycle with a correlation of 0.61. It is interesting to note that this region is characterized by a phase shift between CO-BC and CO-CHEM. As mentioned previously, CO-CHEM is related to production from hydrocarbons emitted within the domain as well as hydrocarbons entering the domain at the lateral boundaries. This phase shift may be explained by the fact that the main part of CO-CHEM comes from precursors from boundary conditions and takes time to be produced. Thus while CO-BC is reduced during transport, CO-CHEM might increase. In the center of the United States (Figure 5d), observed CO mixing ratios are about 200–300 ppbv and WRF-Chem underestimates the CO mixing ratios with a bias of −139 ± 67 ppbv. The strong variability in the observations is not reflected in the model (which can be seen in the poor correlation −0.20). The model values show very little difference from one day to another, while the observations can differ by up to a factor of two. In particular, high CO mixing ratios (up to 500 ppbv) are found in the observations for DOY between 175 and 184, with highest CO especially at the urban sites (not shown here), while the model is significantly lower. These discrepancies might be due to model dilution, transport errors and the model coarse spatial resolution. On a daily basis, the correlation between modeled and observed CO mixing ratios improves (0.74). These results suggest that the model at a coarse spatial resolution better represents the high CO in the western and eastern U.S. regions that are influenced by larger and more densely located pollution sources than in the central United States, where pollution sources are more isolated and for this reason even more diluted in the model.

[26] The mean CO tracer contributions for the different EPA monitoring site categories are presented in Table 3. Averaged over all sites, anthropogenic CO from local sources has the largest contribution with a mixing ratio around 160 ppbv. Because of the medium CO lifetime that allows for significant pollution transport, this is followed by the CO

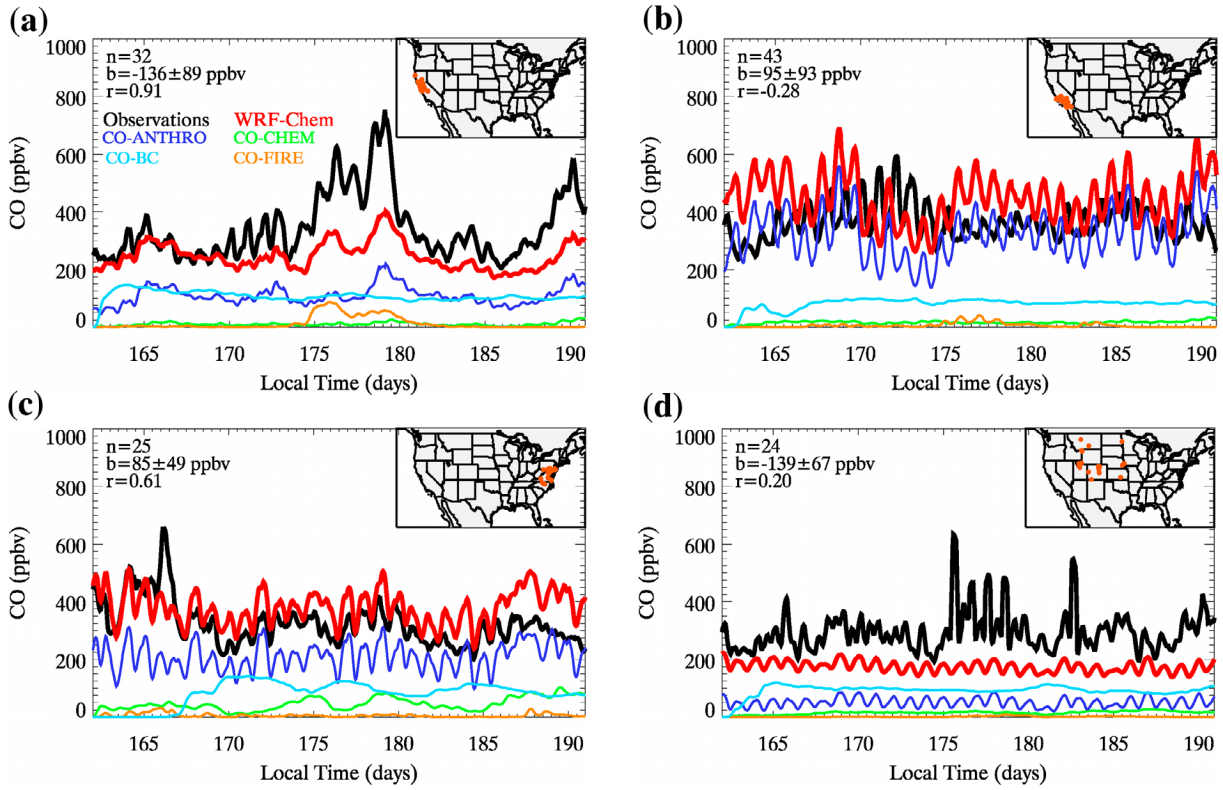

Figure 5. Time series of observed (black) and simulated (red) surface CO averaged over four regions of the United States for the period 10 June to 10 July 2008: (a) Northern California, (b) Southern California, (c) eastern United States, and (d) central United States. Time series are derived by averaging hourly concentrations over a moving 8 h window. Mean bias, associated standard deviation, and correlation coefficient between observed and modeled average time series for the period 24 June to 10 July 2008 are indicated on each graph. WRF-Chem CO tracer time series are also depicted to support the analysis.

inflow (mixing ratio around 93 pbbv). CO produced chemically and from fire contributes to a lesser extent to total CO with mixing ratios of 30 ppbv and 5 ppbv, respectively. However, this may depend on season and vary according to the prevalence of wildfire at any given time. Considering the different types of monitoring sites and the degree to which they are impacted by local or transported pollution, anthropogenic CO has larger contributions at urban sites (mean mixing ratios of 167 ppbv) than at rural sites (mean mixing ratio of 93 ppbv). At rural sites, CO inflow and anthropogenic CO equally contribute to the total CO in absolute terms with a mixing ratio of about 94 ppbv. However, as rural sites have overall lower CO levels, the CO inflow relative contribution is more important at rural (~42%) compared to urban (~30%) environments.

[27] Despite the relatively large grid spacing used in the model, the evaluation at the surface supports our previous findings: the model underestimates CO from fire while it generally overestimates CO from anthropogenic sources, especially over polluted region such as Southern California and the east of the United States.

3.3.2. Specific Case Study

[28] Concentrating now on the comparison at individual monitoring sites, Figure 6 shows the variability of observed and model-simulated surface CO mixing ratio at a rural Washington site (Figure 6, left) and an urban California site (Figure 6, right), together with the CO tracer variability associated with each. Overall, the model reproduces fairly well the variability and magnitude of observed CO mixing ratios, but there are some notable discrepancies.

[29] At the rural site, the observed CO mixing ratios are about 200 ppbv and the model underestimates the CO mixing ratios with a bias of 49 ± 32 ppbv. Modeled and observed time series are indicate an increase in CO around DOY 182, but the increase is less pronounced in the model and over a shorter time span. The observed CO variability also indicates another CO peak around DOY 190 not reflected in the model. The analysis of the CO tracer variability shows that the first increase is related to the fire and anthropogenic tracers. Possible reasons for the modeled

Table 3. Estimates of the Modeled CO Tracer Mixing Ratio Averaged at the Surface Over All and Individual Low-Resolution and High-Resolution EPA Monitoring Site Categories for the Period 24 June to 10 July 2008[a]

EPA Site Categories	CO-CHEM (ppbv)	CO-ANTHRO (ppbv)	CO-FIRE (ppbv)	CO-BC (ppbv)
All	30 ± 8 (29)	160 ± 27 (164)	5 ± 5 (4)	93 ± 7 (93)
Urban	30 ± 8 (29)	167 ± 28 (171)	5 ± 5 (4)	93 ± 7 (93)
Rural	32 ± 10 (30)	93 ± 19 (94)	5 ± 6 (3)	94 ± 8 (93)

[a]Standard deviation is also indicated. Median values are in parentheses.

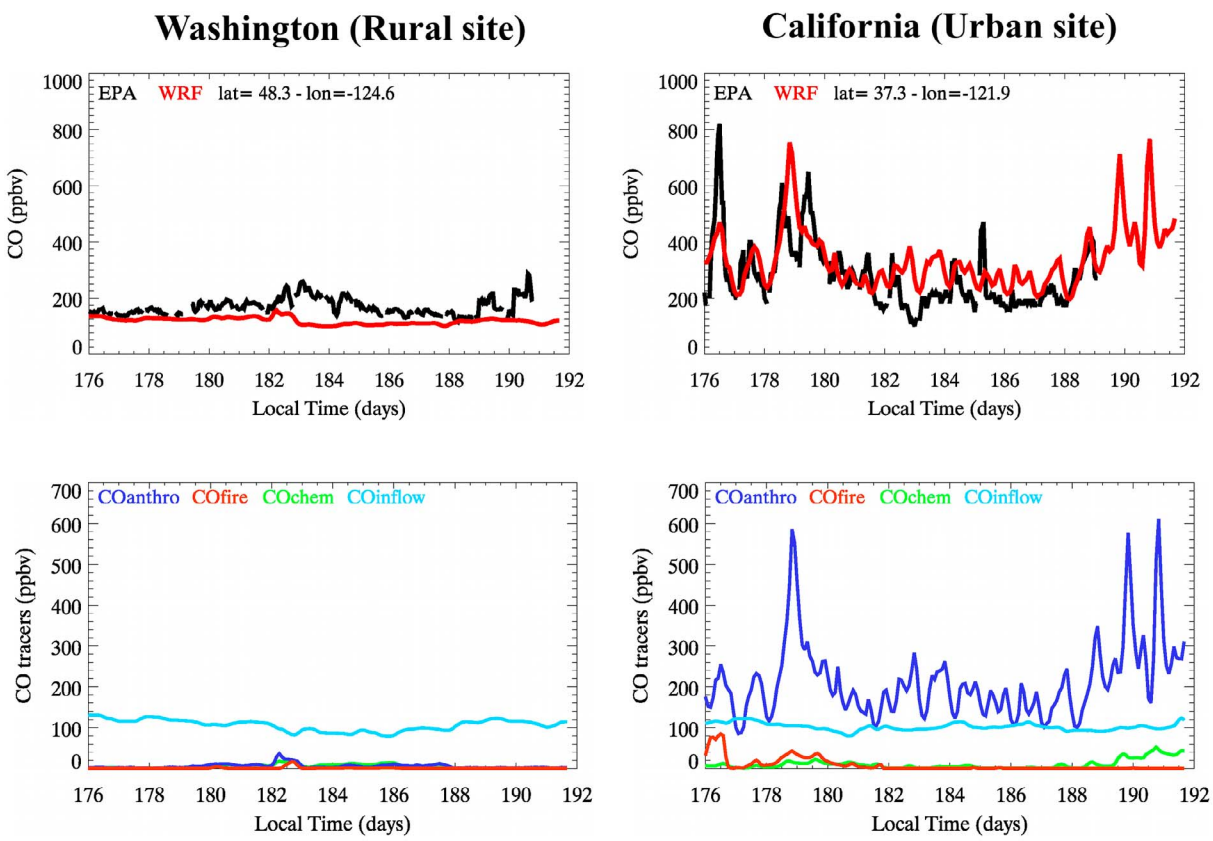

Figure 6. Temporal variability of (top) observed (black) and simulated (red) surface CO and (bottom) CO tracers at (left) a rural site in Washington State (site 530090013) and (right) an urban site in California (site 060850005) for the period 24 June to 10 July 2008.

underestimate are a too small fire and/or anthropogenic source and transport errors. It may also be that compared to the point EPA measurements, the coarser model resolution will tend to smear out and dilute events. While enhanced concentrations are related to regional sources, the dominant source of CO at this site is the pollution inflow.

[30] At the urban site, the surface CO mixing ratios are about 300–400 ppbv with values up to 800 ppbv. This site was under the influence of intense fire plumes during the time period analyzed (as seen by MODIS visible smoke imagery). The CO variability indicates two pronounced peaks during the first part of the simulation period (around DOY 176 and 179). The model suggests that both peaks are linked to fire emissions, and that they are underestimated in the model. The mismatch in the modeled magnitude of the second peak is partly due to an overestimate of anthropogenic emissions, as shown by the CO-ANTHRO time series. The model misses the peak observed around DOY 185 possibly missing some fire plumes that are reaching the site.

4. CO Spatial Distribution and Budget

[31] In this section, we examine the spatial distribution of the different sources of CO over the contiguous United States for the time period 24 June to 10 July 2008. The overall budget of model CO, including CO tracer contributions, is also analyzed.

4.1. CO Spatial Distribution

[32] Figures 7 and 8 illustrate the modeled spatial distribution of total CO and tracer mixing ratios over the United States averaged over the time period 24 June to 10 July 2008 at the surface and for the FT, respectively. The model average FT mixing ratio is derived from the FT column, which is calculated as the gas amount between the top of the model PBL and 8 km. Note that this result is not sensitive to the choice of upper boundary altitude, and similar results are found by defining the FT from model PBL top up to 6 km or 10 km. For the calculation of the mixing ratio averaged over the FT, we normalize the CO column by the air column (integrated over the FT). The total CO is shown in absolute values, while the tracers are shown in terms of relative contributions. In order to help the interpretation, the topography and the PBL height are also depicted in Figures 7 and 8, respectively.

[33] At the surface, the total CO distribution shows highest mixing ratios in the eastern United States (up to around 500 ppbv) and in California with hot spots of CO around Los Angeles (up to 900 ppbv). These elevated CO mixing ratios are due to anthropogenic emissions as evident from the CO-ANTHRO distribution. The CO-FIRE distribution shows that a part of the high CO mixing ratios observed in Northern California and South of the Bay area are related to emissions from wildfires that are transported toward the east and southeast. The CO-CHEM distribution

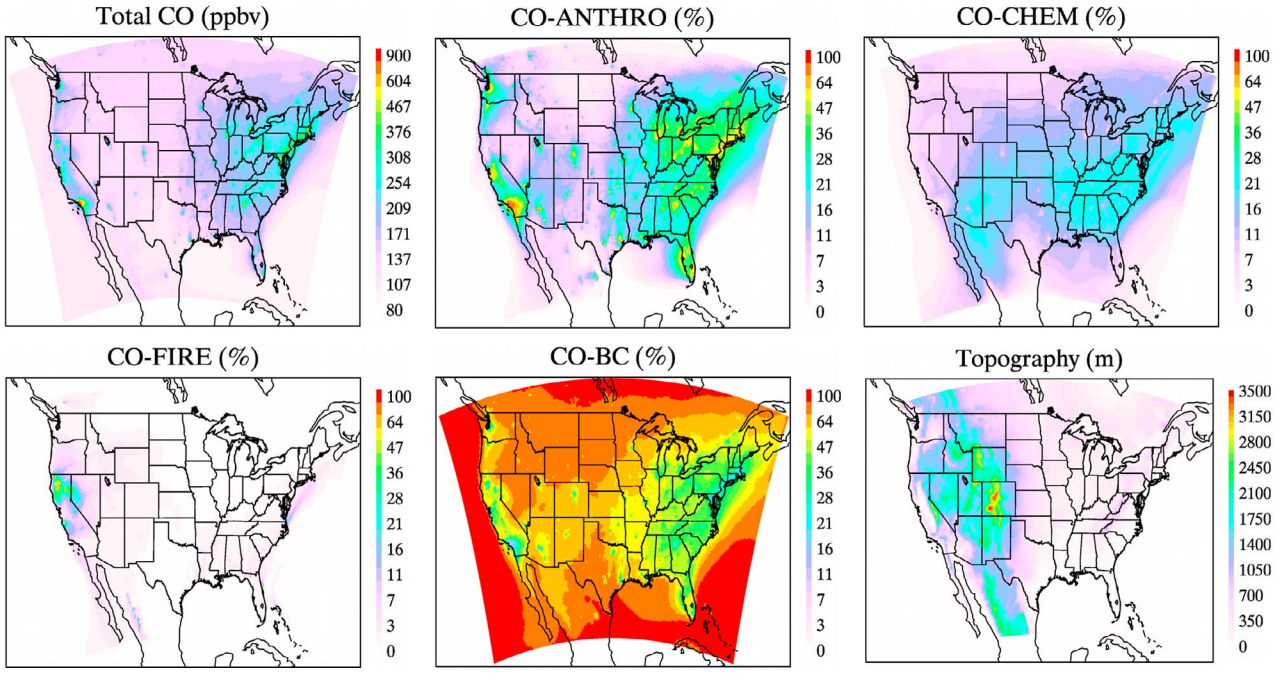

Figure 7. Spatial distributions of total CO mixing ratios (ppbv) and CO tracer relative contributions (%) averaged over the period 24 June to 10 July 2008 at the surface. Note that the color scales are on a logarithmic scale. The surface altitude is also depicted to help the interpretation.

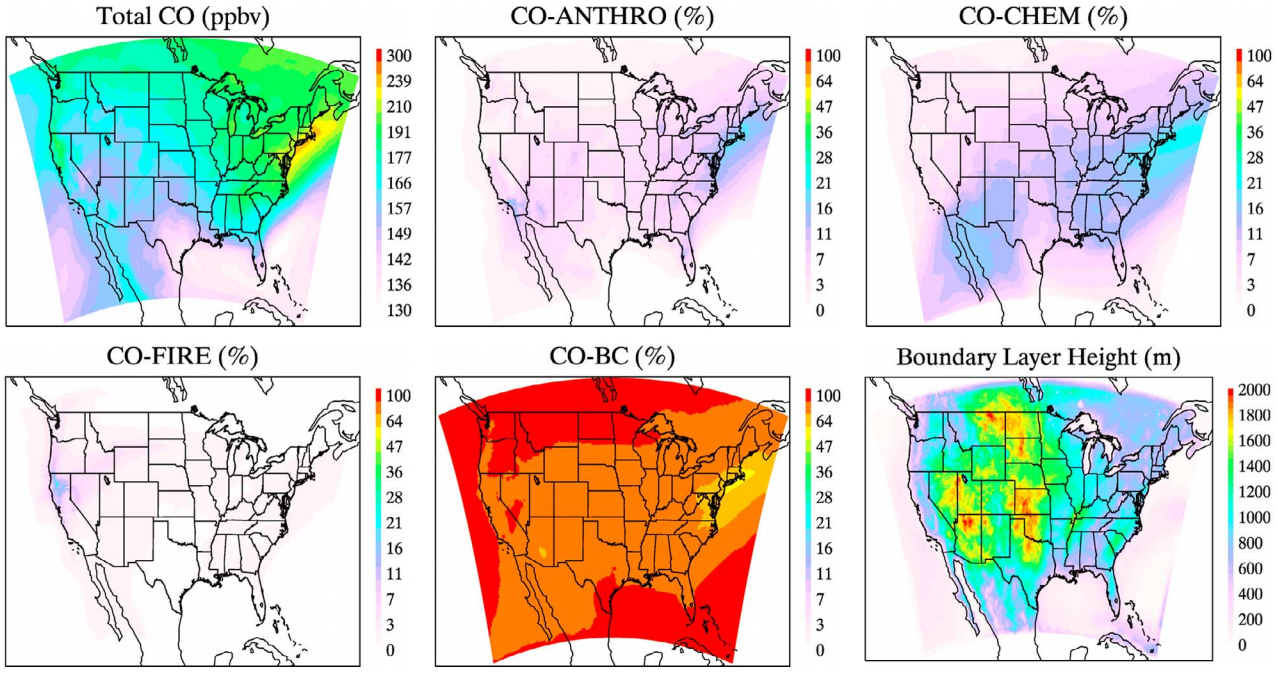

Figure 8. Spatial distributions of total CO mixing ratios (ppbv) and CO tracer relative contributions (%) averaged over the period 24 June to 10 July 2008 in the FT (defined as the CO amount averaged between the top of the PBL and 8 km). Note that the color scales are on a logarithmic scale. The PBL height is also depicted to help the interpretation.

Table 4. Estimates of the CO Mixing Ratio Averaged at the Surface, in the PBL, and in the FT Over the Contiguous United States for the Period 24 June to 10 July 2008[a]

	Average Mixing Ratio Contributions (ppbv)			Average Mixing Ratio Contributions (%)		
	Surface	PBL	FT	Surface	PBL	FT
Total CO	165 ± 68	157 ± 59	116 ± 17			
CO-CHEM	24 ± 19	23 ± 19	10 ± 9	14 ± 8	14 ± 8	9 ± 7
CO-ANTHRO	36 ± 50	29 ± 40	6 ± 6	18 ± 14	15 ± 12	5 ± 4
CO-FIRE	4 ± 24	3 ± 21	2 ± 6	2 ± 5	2 ± 5	1 ± 3
CO-BC	95 ± 20	97 ± 20	96 ± 15	63 ± 19	66 ± 18	84 ± 12

[a]Standard deviation is also indicated. CO tracer contribution values are expressed in both absolute terms (ppbv) and relative terms (%).

shows that photochemical production also adds to the high CO mixing ratios in the eastern United States. The dispersed pattern in CO-CHEM is due to the fact that CO precursors are transported during the time it takes to chemically produce CO. The CO-BC distribution shows that in the western and southern United States, CO mixing ratios are strongly influenced by CO inflow. An interesting feature indicates CO coming from the north, probably owing to intense fires in Canada as were observed by MODIS during this time period (http://rapidfire.sci.gsfc.nasa.gov/firemaps/). In the PBL (not shown here), similar results as those presented at the surface are found.

[34] In the FT, the total CO distribution shows mixing ratios ranging from 80 up to 250 ppbv in the eastern United States. These values are largely due to the pollution inflow as shown in the CO-BC distribution. However, part of total CO mixing ratio is also influenced by anthropogenic CO and CO produced chemically within the domain, especially around the eastern coast of the United States. It is interesting to note that in the FT, photochemically produced CO is more important than anthropogenic CO, while the reverse is the case at the surface. This is largely due to the fact that, in the FT, CO from oxidation of methane is more important than ventilation of anthropogenic CO from the PBL. In addition, many hydrocarbons are long-lived, which likely explains the higher contribution of photochemically produced CO downwind of the northeast in the FT. However, isoprene, which is a short-lived species, might contribute significantly to the surface budget of photochemically produced CO, for example, explaining the higher contribution of photochemically produced CO at the surface over the southeast. Models might also underestimate the venting of pollution out of the PBL into the FT as was shown by *Castellanos et al.* [2011] for this region. The CO-FIRE distribution shows that the wildfire emissions at the surface can be transported vertically up to the FT, followed by transport toward the east and north. These results show higher correlation between the surface and the FT in the vicinity of strong sources.

4.2. PBL and FT CO Budget Comparison

[35] We first analyze the CO burden integrated over the PBL and over the FT. On average, the daily CO burden over the contiguous United States for the time period June 24 to July 10 2008 is about 1.30 Tg CO for the PBL and 3.97 Tg CO for the FT. The CO inflow boundary conditions contribute up to 63% in the PBL and up to 84% in the FT. Contrary to this, for anthropogenic and chemical sources, higher contributions are found in the PBL compared to the FT (CO-ANTHRO explain 15% of the CO burden compared to 5% and CO-CHEM explain 14% compared to 9%). With fire sources, similar contributions are found in both the PBL and the FT with a mean contribution of about 1–2%. Over the analysis time period, the total CO burden amounts show little day-to-day variability (standard deviation is around 0.013 Tg in the PBL and 0.023 Tg in the FT).

[36] The calculated burden amounts are influenced by the variation of the PBL height, and we examine the average mixing ratios of CO and CO tracers in the PBL and in the FT (Table 4). At the surface, the average mixing ratio of total CO over the contiguous United States is estimated as 165 ± 68 ppbv. A similar value is found in the PBL (157 ± 59 ppbv) while a lower value is found in the FT (116 ± 17 ppbv). The surface average mixing ratios of CO tracers are calculated as 24 ± 19 ppbv for CO-CHEM, 36 ± 50 ppbv for CO-ANTHRO, 4 ± 24 pbbv for CO-FIRE and 95 ± 20 ppbv for CO-BC. Similar mixing ratios are found in the PBL, while lower mixing ratios are found in the FT, in particular for CO-CHEM (10 ± 9 ppbv), CO-ANTHRO (6 ± 6 ppbv) and CO-FIRE (2 ± 5 ppbv). The CO-BC average mixing ratio is of the same order of magnitude at the surface (95 ± 20 ppbv), in the PBL (97 ± 20 ppbv) and in the FT (96 ± 15 ppbv). However, the relative mixing ratio contribution shows a larger influence of CO-BC in the FT (84 ± 12%), compared to the surface (63 ± 19%) and the PBL (66 ± 18%).

5. CO Vertical Distribution

[37] Section 4 was focused on the analysis of the horizontal distribution of CO over the United States. We now turn to the vertical distribution of CO and use simulated CO and CO tracers to understand the influence of different sources. To address this, we analyze the CO vertical and temporal structure for highly polluted regions over the United States.

[38] Figure 9a shows the locations with the highest 10% of modeled surface CO mixing ratios over the United States (a map of CO emissions is also provided in Figure 9b to indicate the source locations). The selection of the highest CO regions is based on the temporal median of each model grid cell. On average for the highest CO sites, surface emissions are in the range of 160 ± 100 mol km^{-2} h^{-1}. High CO regions are around urban areas and most densely concentrated over the eastern United States as shown in Figure 9a. From these, we select one area on the East Coast with high CO considered as representative of polluted regions. This area is delimited by a blue rectangle in Figure 9a. Note that we only select grid cells within the blue box that are similar in elevation (lower than 500 m).

[39] Figure 10 (left) illustrates the temporal and vertical distributions of total CO and CO tracer mixing ratios averaged over the selected region. The average PBL height is also included in each plot (dashed black line). In the FT, the total CO mixing ratios are around 100–150 ppbv, while in the PBL the mixing ratios are double (200–300 ppbv). In this layer, the total CO mixing ratios are characterized by a strong diurnal cycle, also seen in the CO-ANTHRO plot and to a lesser extent in the CO-CHEM plot, reflecting diurnal variations in the PBL height, emissions and photochemistry. For the first 10 days of the simulation period, the model

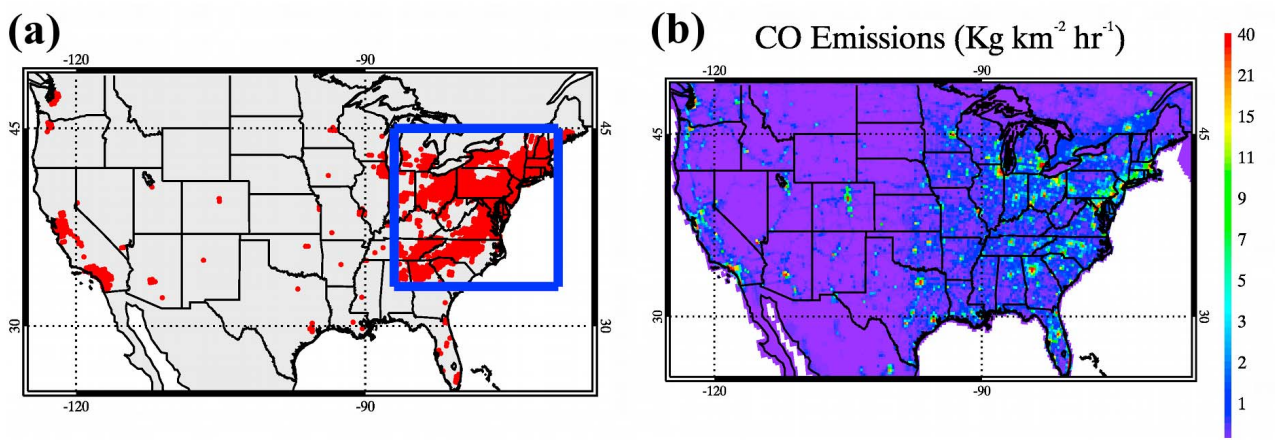

Figure 9. (a) Locations of the surface sites with highest CO mixing ratios. (b) Spatial distribution of CO emissions.

shows strong vertical gradients within the PBL, which is partly due to the presence of clouds during that time period and the PBL scheme used in WRF-Chem that underestimates the vertical mixing [*Hu et al.*, 2010]. This strong vertical gradient within the nominal PBL averaged over the East Coast of the United States may make a comparison with surface sites challenging at best. The cross section distribution for CO-BC shows episodic low-altitude transport, probably due to Canadian emissions, increasing the surface CO by ~100 ppbv. Note that the Canadian emissions include the anthropogenic and fire emissions used in MOZART-4 simulations that serve as boundary conditions. During the simulation time period, fire emissions in this region have little influence on total CO (not shown here).

[40] Figure 10 (right) shows the time series of CO and CO tracer mixing ratios at the surface and at different altitude levels representative of the PBL (1 km) and the FT (2 and 3 km). The plot of surface and 1 km CO variability, characterized by amplitude of 100–200 ppbv, highlights the fine diurnal-scale temporal variability, as discussed in Figure 10 (left), but also a larger-scale variability associated with variations in emissions and chemistry. These fine- and large-scale variations seen in the PBL have only a weak influence in the FT, with amplitude less than 50 ppbv, because of the variability in FT chemically produced CO. In addition, FT CO-BC mixing ratios also contribute to a part of the large-scale variability observed in FT total CO (amplitude of ~50 ppbv). These results show that different processes determine the variability at the surface and in the FT and there is no clear correlation between the surface and the FT variations.

6. Air Quality Monitoring From Satellite Observations

[41] Air pollution monitoring is currently primarily based on surface networks that have good temporal, but limited spatial coverage and no information about the atmospheric vertical distribution or indeed the atmospheric column analyzed in section 4. In recent years, satellite observations have been used for studying tropospheric composition. Satellites provide good long-term spatial coverage with some vertical profile information, but the question arises as to the extent to which satellite retrievals can be used to infer information on the surface concentrations for AQ applications. Possible applications where satellite retrievals could be tremendously helpful for are, for example, the monitoring of emission trends, deriving information about pollution transport on small and large scale or estimating the degree of lofting of pollution out of the PBL. In this section, we discuss the sensitivity of the currently available classes of satellite CO retrievals to the near-surface CO concentrations.

6.1. Sensitivity of the Current CO Satellite Measurements

[42] Currently, CO retrievals from passive nadir satellite measurements are based on two different wavelength ranges: the TIR surface and atmospheric emission with primary sensitivity to the FT partial column, and the NIR solar backscattered radiances with sensitivity to the total column. Since CO is mainly concentrated in the troposphere, we define the CO total column as the integrated column corresponding to the lowermost 8 km of the troposphere above surface level.

[43] Retrievals that use only the NIR signals such as SCIAMACHY (Scanning Imaging Absorption Spectrometer for Atmospheric Chartography) [*Buchwitz et al.*, 2004; *Piters et al.*, 2006] and some MOPITT products provide CO measurements that are typically sensitive to the total column [*Buchwitz et al.*, 2004, 2007; *Deeter et al.*, 2009]. The question then arises: are these measurements sufficiently precise to capture what happens in the lowermost part of the troposphere? It has been demonstrated that the NO_2 total column retrievals are a reasonable indication of the amount of NO_2 present in the PBL [e.g., *Blond et al.*, 2007] as this molecule has a very short lifetime and generally never gets out the PBL, and when it does, is almost immediately oxidized. The measurement of NO_2 total column is therefore useful for AQ applications [*Herron-Thorpe et al.*, 2010; *Zyrichidou et al.*, 2009]. To determine if the CO total column is similarly representative of surface or PBL CO concentrations, we investigate how much of the CO total column is contained in the LMT. Since satellite retrievals are primarily sensitive to atmospheric pressure, and do not track the evolution of the PBL height, consideration of the LMT column (defined here as the partial column corresponding to

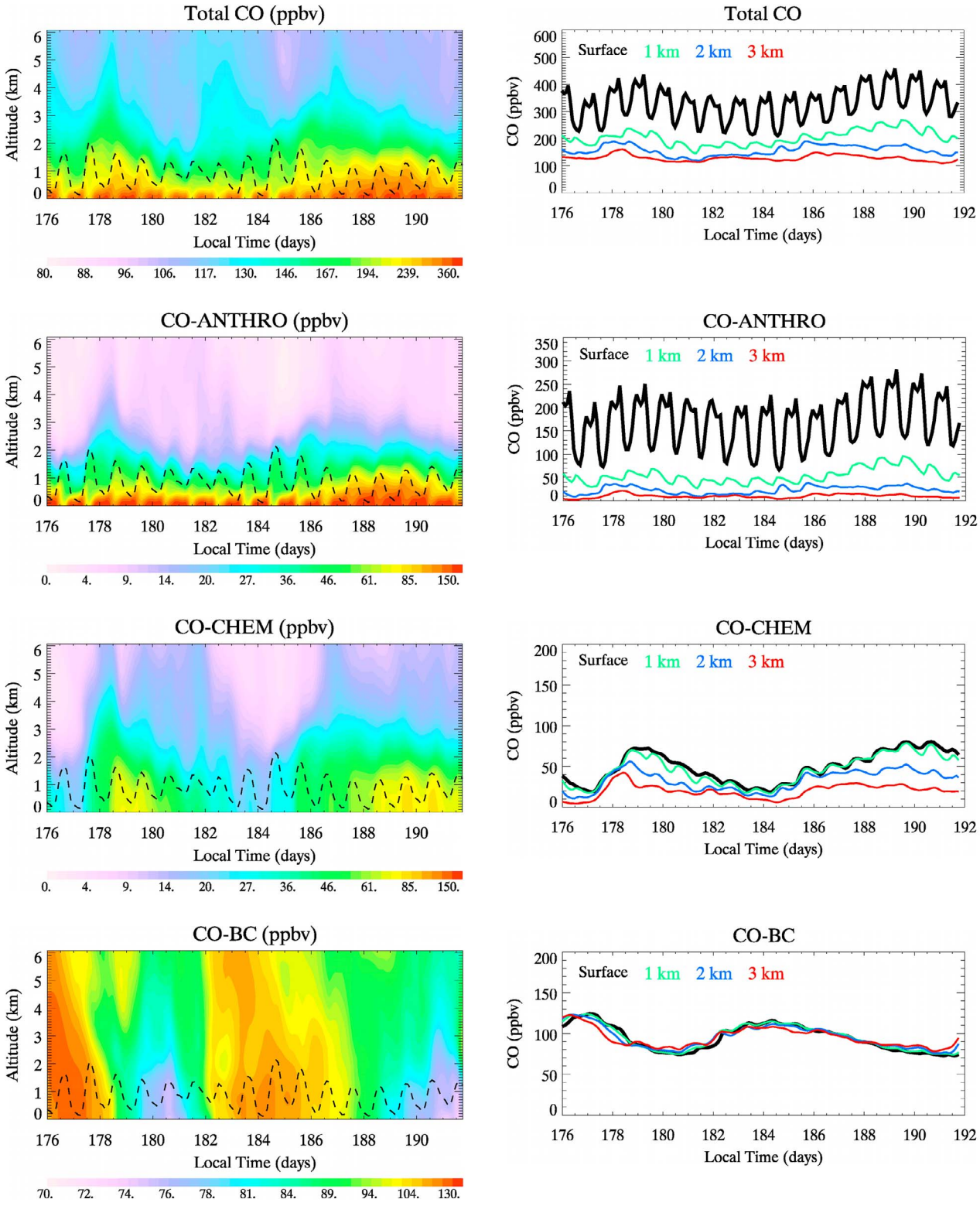

Figure 10. (left) Altitude-time cross sections of total CO and CO tracer mixing ratios for the period 24 June to 10 July 2008, averaged over the East Coast area considered as a polluted region. Note that the color scales are on a logarithmic scale and differ among the graphs. (right) Associated time series of CO and CO tracer mixing ratios for the surface and for different altitudes (1, 2, and 3 km).

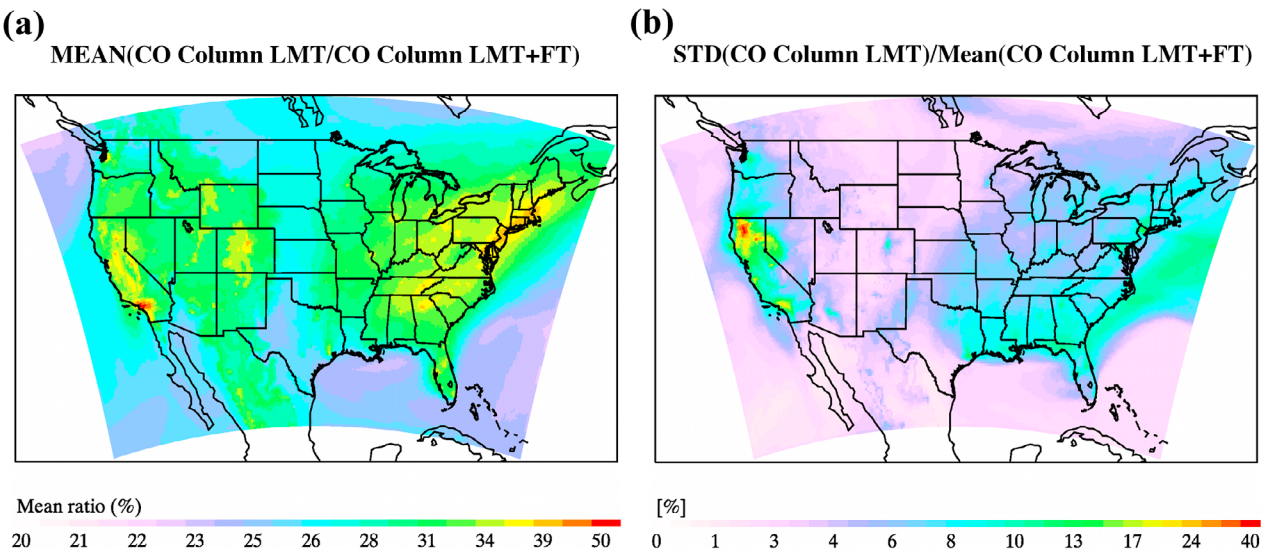

Figure 11. (a) Time-average ratio between CO LMT column and CO LMT + FT column in percent for the period 24 June to 10 July 2008. (b) Ratio between the standard deviation (STD) of CO LMT column and the time average of CO LMT + FT in percent.

the lowermost 150 hPa of the troposphere above surface level) is more appropriate than the PBL column amount.

[44] Figure 11a illustrates the distribution of the mean fraction of the CO LMT partial column to the CO total column. In the eastern United States and in Northern California, impacted by anthropogenic and fire emissions, respectively, around 30–40% of the CO total column is in the LMT, and in Los Angeles and the Washington, D. C.–Boston metropolitan corridor, up to 50% of the CO total column is in the LMT. This shows that CO total column is not necessarily dominated by the CO LMT contribution, while sensitivity to this part of the atmosphere is of most interest for AQ applications. Thus a measurement of CO total column cannot be reliably used as a proxy for the LMT or PBL column as it can for NO_2. This is due to the longer lifetime of CO, and the fact that CO does get out the PBL and undergoes long-range transport. This is illustrated by the impact of CO-BC on the CO distribution and budget described in section 4.

[45] We subsequently quantify the sensitivity that would be needed in the case of a CO total column measurement in order to pick up the variation in the LMT partial column that we are interested in for AQ applications. Figure 11b illustrates the distribution of the ratio between the standard deviation of the CO LMT partial column and the mean CO total column. In very polluted cases such as in Northern California impacted by fire emission, the variability in the LMT can be high (up to 35%) but for usual anthropogenic cases (such as in the eastern United States), the variability in the LMT is about 10%. In order to catch the variability in the LMT, a measurement precision significantly better than 10% would be required, which is less than current satellite CO column measurement retrieval error [e.g., *de Laat et al.*, 2010]. Thus current retrieval performance would have to be significantly improved to make a total column measurement suitable for AQ applications.

[46] The current TIR satellite sensors measuring CO are MOPITT [*Deeter et al.*, 2003], Atmospheric Infrared Sounder (AIRS) [*Warner et al.*, 2007], Tropospheric Emission Spectrometer (TES) [*Rinsland et al.*, 2006], and Infrared Atmospheric Sounding Interferometer (IASI) [*Clerbaux et al.*, 2009]. The TIR retrievals rely strongly on thermal contrast, defined as the difference between the surface and the lower atmospheric temperature, and lead in general to low sensitivity to the surface and high sensitivity to the FT [*Deeter et al.*, 2004; *George et al.*, 2009; *Luo et al.*, 2007; *Warner et al.*, 2007]. Under conditions of strong thermal contrast, which is not the general case, TIR retrieval sensitivity to lower troposphere increases [*Clerbaux et al.*, 2008; *Deeter et al.*, 2007].

[47] As mentioned above, NIR-only and TIR-only measurements, for different reasons, provide limited information about the lowermost part of the troposphere. Increased sensitivity to near-surface CO concentrations from multispectral (TIR+NIR) retrievals has been shown by satellite OSSEs [*Edwards et al.*, 2009]. Recently the MOPITT team has made significant advances in demonstrating multispectral retrievals of CO with enhanced sensitivity to near-surface CO [*Deeter et al.*, 2011; *Worden et al.*, 2010]. This new product has recently been made available to the community and will be used in future studies. In the following analysis, we examine the ability of multispectral retrievals to capture variations in LMT CO concentrations.

6.2. Case Study

[48] In this section, we focus on one specific polluted case located in Washington D.C. in order to assess the extent to which satellite measurements are able to capture the variability that happens in the PBL or at the surface. To simplify the analysis, we use the total column average mixing ratio as a proxy for an NIR retrieval, the FT average mixing ratio as a proxy for the TIR retrieval, and the LMT average mixing ratio as a proxy for the multispectral (TIR + NIR) retrieval.

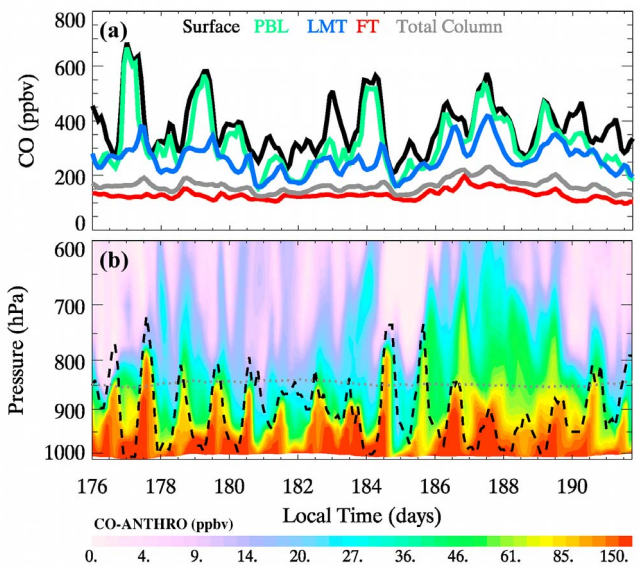

Figure 12. (a) Time series of CO average mixing ratios at the surface and in different columns (PBL, LMT, FT, and total column) for the period 24 June to 10 July 2008 in Washington D. C. (b) Associated altitude-time cross sections of CO anthropogenic tracer mixing ratios. The black dashed line represents the boundary layer height, and the gray dotted line represents the altitude corresponding to the lowermost 150 hPa of the troposphere (surface to the altitude corresponding to surface pressure −150 hPa). Note that the color scale is on a logarithmic scale.

These proxies are similar to assuming constant averaging kernels as would be appropriate for the general case with low thermal contrast and reasonably high and constant surface reflectivity. Although ignoring the scene-by-scene variation in the averaging kernel due to heterogeneous surface conditions is an obvious limitation, we do not expect it to alter the main conclusions.

[49] Figure 12 illustrates the variability of different CO partial column average mixing ratios (Figure 12a) and the time-altitude cross section of anthropogenic CO (Figure 12b) in Washington DC. The PBL height and the top of our defined LMT are also displayed in Figure 12b in dashed black lines and dotted gray lines, respectively. Note that as anthropogenic CO is the dominant source of CO here, we only show the CO-ANTHRO cross-section plot.

[50] Figure 12a shows that the surface CO average mixing ratio peaks in the very early morning after the PBL collapse. Surface and PBL CO average mixing ratios generally track except at night when the PBL is stably stratified, which leads to a strong CO gradient through the PBL (e.g., around DOY 176 or 182). Note that around DOY 180.5 (i.e., during daytime), surface and PBL CO mixing ratios do not track, which is probably due to the PBL scheme used in WRF-Chem that underestimates the vertical mixing [*Hu et al.*, 2010]. This shows that the PBL average mixing ratio can be a good measure of the surface mixing ratios when CO mixing ratios are well mixed up in the PBL (usually during daytime), which is due to ground-level heating, but not if a strong vertical CO gradient is present (usually during nighttime).

[51] During daytime when the PBL is higher than the top of the LMT (around 850 hPa), the PBL CO average mixing ratio and the LMT CO average mixing ratio (the multispectral NIR + TIR retrieval proxy) are close (e.g., around DOY 185.5). This is generally the case in presence of high temperatures leading to a strong vertical mixing. In contrast, when the PBL height is very low and the surface mixing ratio reaches a maximum, generally at night, the LMT partial column average mixing ratio can be quite different from the PBL mixing ratio. However, LMT column measurements will not in any case be available during the night in absence of the NIR reflected solar measurement in the multispectral retrievals.

[52] The FT CO average mixing ratio (the TIR retrieval proxy) in general does not follow the surface variability. It is, however, sensitive to concentration changes due to long-range transport (as shown in section 4). As a consequence, the FT column may be used to specify the model initial and boundary conditions, which is a use of the current satellite TIR measurements. The total column average mixing ratio (the NIR retrieval proxy) variation shows poor sensitivity to surface mixing ratio as discussed in section 6.1.

[53] Table 5 gives the statistics between the surface CO mixing ratios and the integrated LMT, FT and total column average mixing ratio for Washington DC. Owing to dilution as a result of vertical mixing, the partial column average mixing ratio is usually lower than the surface mixing ratio. As expected, good statistics are found between the surface and the PBL (bias of 54 ± 37 ppbv, RMSE of 65 ppbv and correlation coefficient of 0.91). Similar results are found between the surface and the LMT. Although we have a reasonable correlation between the surface and the total column (0.61), the bias and RMSE are very high (185 ppbv and 200 ppbv, respectively). This shows that the total column is not useful to capture surface absolute concentrations. The highest bias and RMSE (222 ppbv and 237 ppbv, respectively) and the lowest correlation coefficient (0.38) are found between the surface and the FT CO mixing ratios as this is the only measure that is not sensitive to the lower troposphere. This shows that the surface and FT CO are not well correlated but that the LMT column has potential to provide some information about surface AQ. Note that our estimates in Table 5 are conservative given that the model shows less variability than the observations.

7. Conclusions

[54] We have assessed the CO budget and spatiotemporal variability over the contiguous United States using the

Table 5. Key Statistics With Respect to the Surface CO Mixing Ratios in Washington, D. C., for the Period 24 June to 10 July 2008[a]

	Bias (ppbv)	RMSE (ppbv)	Correlation Coefficient
Surface-PBL	54 ± 37	65	0.91
Surface-LMT	77 ± 61	98	0.74
Surface-FT	222 ± 84	237	0.38
Surface-total column	185 ± 77	200	0.61

[a]The mean absolute bias, standard deviation, root mean square error (RMSE), and correlation coefficient are given.

regional chemistry transport model WRF-Chem V3.2. In the framework of this study, four CO tracers, including tracers from anthropogenic and fire emissions, photochemical CO production from within the domain and CO transported into the regional domain from the lateral boundaries were set up in the model. Using CO tracers is valuable for tracking CO emitted from individual emission sources and thus to better understand the different factors driving CO variations at the scale of interest to AQ applications. To our knowledge, the use of CO tracers in a regional model is an innovative aspect of this work.

[55] The main conclusions of this work may be summarized as follows.

1. Model evaluation results combining aircraft, satellite, and surface observations showed a good agreement between the model and the observations, but pointed out an underestimate of fire emissions, an overestimate of anthropogenic emissions especially over Southern California and the east of the United States and a positive bias in pollution inflow. We also showed that the model gives a fairly good representation of background CO mixing ratios over the entire altitude range.

2. Over the contiguous United States, for the entire altitude range, the largest CO contribution is transported pollution with a mean relative contribution ranging from 60% at the surface and in the PBL to 80% in the FT. Chemical and anthropogenic sources contribute to a lesser extent (14% and 18% at the surface and in the PBL, and 9% and 5% in the FT, respectively). Fire emissions make a small contribution to mean CO at all altitudes (<4%) but its contribution is regionally and event dependent.

3. In polluted regions, the surface and PBL CO mixing ratios both show strong diurnal variability, owing to the diurnal variations of the PBL height, emissions and photochemistry, and larger-scale variability due to the variations in emissions and chemistry, which are not reflected higher up in the FT. This shows that different processes determine the variability at the surface and in the FT and there is no clear correlation between what happens at the surface and what happens in the lower FT.

4. We compared the representation of surface and PBL CO concentration variability that would be captured by representative satellite sensor observations using the different CO spectral bands: NIR radiances mostly sensitive to the total column, TIR mainly sensitive to the FT column and multispectral NIR+TIR radiances that provide sensitivity to the LMT column. We found that a measurement of CO LMT column represents on average ~30% of the total column. This implies the CO total column variation cannot easily be used as a proxy for that of the LMT as it can be for NO_2, for example. This is particularly due to the longer lifetime of CO and thus the fact that CO can get lofted out of the PBL and is transported over large distances. We also found that for a typical polluted urban scenario, the variability of CO in the LMT is on the order of 10% of the total column amount, which is of the order of actual satellite CO column retrieval errors. Thus the current performance of CO satellite retrievals would have to be significantly improved upon to make a total column measurement suitable for AQ applications.

5. The PBL partial column can be a good representation of the surface concentration, especially when CO is well mixed in the PBL, which usually occurs during daytime as a result of ground-level heating. However, since retrievals are sensitive to atmospheric pressure and do not track changes in PBL height, consideration of the concentration in the LMT, below a certain pressure, is more appropriate than that of the PBL. During daytime and when the PBL is higher than the top of the LMT, PBL and LMT CO average mixing ratios are close. On the contrary, the concentrations can differ considerably at night when the PBL height is very low. Our results show that during daytime, when higher temperatures lead to a strong vertical mixing and a high PBL height, the LMT concentration that can be retrieved with multispectral NIR + TIR observations is a good measure of that in the PBL.

6. The FT CO average mixing ratio (representative of a TIR retrieval) in general does not follow the surface variability. However, it is a good measurement for capturing the pollution inflow variability and therefore, is valuable for informing about initial and boundary conditions to constrain regional models.

[56] The results of this study demonstrate that for AQ monitoring, satellite products with increased sensitivity toward the surface are needed. The new MOPITT V5 multispectral CO retrieval shows real sensitivity at the surface and is capable of a meaningful surface retrieval of CO concentration [*Deeter et al.*, 2011; *Worden et al.*, 2010]. This product has recently been made available to the community as a beta release and the new data product will be examined in future work after it has been validated. Building on this development, we are exploring the use of this new technique for AQ retrievals of CO and ozone from the next-generation of geostationary satellite missions such as the GEO-CAPE mission.

[57] **Acknowledgments.** The authors would like to thank Stu McKeen (NOAA ESRL) for support with the EPA NEI 2005 emission inventory, the U.S. Environmental Protection Agency (EPA Air Quality System (AQS)) for providing surface monitoring data, and Christine Wiedinmyer (NCAR/ACD) for providing us with fire emissions. We further acknowledge Louisa Emmons and Steve Massie (NCAR/ACD) for their very useful comments on the manuscript and three anonymous reviewers for highly valuable manuscript input. The authors acknowledge the ARC-TAS science team and the START08 project for access to aircraft data. We also acknowledge the strong support of the European Commission, Airbus, and the airlines (Lufthansa, Austrian, and Air France) who carry free of charge the MOZAIC equipment and who have performed the maintenance since 1994. MOZAIC is presently funded by INSU-CNRS (France), Meteo-France, and Forschungszentrum (FZJ, Julich, Germany). The MOZAIC database is supported by ETHER (CNES and INSU-CNRS). This work is supported by NASA grants NNX11AI10G, NNX11AI51G, and NNX09AH03G. NCAR is operated by the University Corporation for Atmospheric Research under the sponsorship of the National Science Foundation.

References

Badr, O., and S. D. Probert (1994), Carbon monoxide concentration in the Earth's atmosphere, *Appl. Energy*, *49*, 99–143, doi:10.1016/0306-2619(94)90035-3.

Bey, I., D. J. Jacob, R. M. Yantosca, J. A. Logan, B. D. Field, A. M. Fiore, Q. Li, H. Y. Liu, L. J. Mickley, and M. G. Schultz (2001), Global modeling of tropospheric chemistry with assimilated meteorology: Model description and evaluation, *J. Geophys. Res.*, *106*, 23,073–23,095, doi:10.1029/2001JD000807.

Blond, N., K. F. Boersma, H. J. Eskes, R. J. van der A M. Van Roozendael, I. De Smedt, G. Bergametti, and R. Vautard (2007), Intercomparison of SCIAMACHY nitrogen dioxide observations, in situ measurements and air quality modeling results over western Europe, *J. Geophys. Res.*, *112*, D10311, doi:10.1029/2006JD007277.

Buchwitz, M., et al. (2004), Global carbon monoxide as retrieved from SCIAMACHY by WFM-DOAS, *Atmos. Chem. Phys.*, *4*, 1945–1960, doi:10.5194/acp-4-1945-2004.

Buchwitz, M., I. Khlystova, H. Bovensmann, and J. P. Burrows (2007), Three years of global carbon monoxide from SCIAMACHY: Comparison with MOPITT and first results related to the detection of enhanced CO over cities, *Atmos. Chem. Phys.*, *7*, 2399–2411, doi:10.5194/acp-7-2399-2007.

Castellanos, P., L. T. Marufu, B. G. Doddridge, B. F. Taubman, J. J. Schwab, J. C. Hains, S. H. Ehrman, and R. R. Dickerson (2011), Ozone, oxides of nitrogen, and carbon monoxide during pollution events over the eastern United States: An evaluation of emissions and vertical mixing, *J. Geophys. Res.*, *116*, D16307, doi:10.1029/2010JD014540.

Chin, M., D. Jacob, J. Munger, D. Parrish, and B. Doddridge (1994), Relationship of ozone and carbon monoxide over North America, *J. Geophys. Res.*, *99*, 14,565–14,573, doi:10.1029/94JD00907.

Chin, M., P. Ginoux, S. Kinne, B. N. Holben, B. N. Duncan, R. V. Martin, J. A. Logan, J. Higurashi, and T. Nakajima (2002), Tropospheric aerosol optical thickness from the GOCART model and comparisons with satellite and Sun photometer measurements, *J. Atmos. Sci.*, *59*, 461–483, doi:10.1175/1520-0469(2002)059<0461:TAOTFT>2.0.CO;2.

Chou, M.-D., and M. J. Suarez (1994), An efficient thermal infrared radiation parameterization for use in general circulation models, *NASA Tech. Memo., TM-104606*, 85 pp.

Clerbaux, C., D. P. Edwards, M. Deeter, L. Emmons, J.-F. Lamarque, X. X. Tie, S. T. Massie, and J. Gille (2008), Carbon monoxide pollution from cities and urban areas observed by the Terra/MOPITT mission, *Geophys. Res. Lett.*, *35*, L03817, doi:10.1029/2007GL032300.

Clerbaux, C., et al. (2009), Monitoring of atmospheric composition using the thermal infrared IASI/MetOp sounder, *Atmos. Chem. Phys.*, *9*, 6041–6054, doi:10.5194/acp-9-6041-2009.

Crutzen, P. (1973), Discussion of chemistry of some minor constituents in stratosphere and troposphere, *Pure Appl. Geophys.*, *106*, 1385–1399, doi:10.1007/BF00881092.

Crutzen, P. J., and P. H. Zimmermann (1991), The changing photochemistry of the troposphere, *Tellus, Ser. B*, *43*, 136–151.

Daniel, J. S., and S. Solomon (1998), On the climate forcing of carbon monoxide, *J. Geophys. Res.*, *103*, 13,249–13,260, doi:10.1029/98JD00822.

Deeter, M. N., et al. (2003), Operational carbon monoxide retrieval algorithm and selected results for the MOPITT instrument, *J. Geophys. Res.*, *108*(D14), 4399, doi:10.1029/2002JD003186.

Deeter, M. N., L. K. Emmons, D. P. Edwards, J. C. Gille, and J. R. Drummond (2004), Vertical resolution and information content of CO profiles retrieved by MOPITT, *Geophys. Res. Lett.*, *31*, L15112, doi:10.1029/2004GL020235.

Deeter, M. N., D. P. Edwards, J. C. Gille, and J. R. Drummond (2007), Sensitivity of MOPITT observations to carbon monoxide in the lower troposphere, *J. Geophys. Res.*, *112*, D24306, doi:10.1029/2007JD008929.

Deeter, M. N., D. P. Edwards, J. C. Gille, and J. R. Drummond (2009), CO retrievals based on MOPITT near-infrared observations, *J. Geophys. Res.*, *114*, D04303, doi:10.1029/2008JD010872.

Deeter, M. N., et al. (2010), The MOPITT version 4 CO product: Algorithm enhancements, validation, and long-term stability, *J. Geophys. Res.*, *115*, D07306, doi:10.1029/2009JD013005.

Deeter, M. N., H. M. Worden, J. C. Gille, D. P. Edwards, D. Mao, and J. R. Drummond (2011), MOPITT multispectral CO retrievals: Origins and effects of geophysical radiance errors, *J. Geophys. Res.*, *116*, D15303, doi:10.1029/2011JD015703.

de Laat, A. T. J., et al. (2010), Validation of five years (2003–2007) of SCIAMACHY CO total column measurements using ground-based spectrometer observations, *Atmos. Meas. Tech.*, *3*, 1457–1471, doi:10.5194/amt-3-1457-2010.

Duncan, B. N., and J. A. Logan (2008), Model analysis of the factors regulating the trends and variability of carbon monoxide between 1988 and 1997, *Atmos. Chem. Phys.*, *8*, 7389–7403, doi:10.5194/acp-8-7389-2008.

Edgerton, E. S., B. E. Hartsell, R. D. Saylor, J. J. Jansen, D. A. Hansen, and G. M. Hidy (2005), The Southeastern Aerosol Research and Characterization Study: Part II - Filter-based measurements of fine and coarse particulate matter mass and composition, *J. Air Waste Manage. Assoc.*, *55*, 1527–1542.

Edgerton, E. S., B. E. Hartsell, R. D. Saylor, J. J. Jansen, D. A. Hansen, and G. M. Hidy (2006), The Southeastern Aerosol Research and Characterization Study: Part III - Continuous measurements of PM2.5 mass and composition, *J. Air Waste Manage. Assoc.*, *56*, 1325–1341.

Edwards, D. P., et al. (2006), Satellite observed pollution from Southern Hemisphere biomass burning, *J. Geophys. Res.*, *111*, D14312, doi:10.1029/2005JD006655.

Edwards, D. P., A. F. Arellano, and M. N. Deeter (2009), A satellite observation system simulation experiment for carbon monoxide in the lowermost troposphere, *J. Geophys. Res.*, *114*, D14304, doi:10.1029/2008JD011375.

Emmons, L. K., G. G. Pfister, D. P. Edwards, J. C. Gille, G. Sachse, D. Blake, S. Wofsy, C. Gerbig, D. Matross, and P. Nédélec (2007), Measurements of Pollution in the Troposphere (MOPITT) validation exercises during summer 2004 field campaigns over North America, *J. Geophys. Res.*, *112*, D12S02, doi:10.1029/2006JD007833.

Emmons, L. K., D. P. Edwards, M. N. Deeter, J. C. Gille, T. Campos, P. Nédélec, P. Novelli, and G. Sachse (2009), Measurements of Pollution in the Troposphere (MOPITT) validation through 2006, *Atmos. Chem. Phys.*, *9*, 1795–1803, doi:10.5194/acp-9-1795-2009.

Emmons, L. K., et al. (2010), Description and evaluation of the Model for Ozone and Related chemical Tracers, version 4 (MOZART-4), *Geosci. Model Dev.*, *3*, 43–67, doi:10.5194/gmd-3-43-2010.

Freitas, S. R., K. M. Longo, R. Chatfield, R. Latham, M. A. S. Silva Dias, M. O. Andreae, E. Prins, J. C. Santos, R. Gielow, and J. A. Carvalho Jr. (2007), Including the sub-grid scale plume rise of vegetation fires in low resolution atmospheric transport models, *Atmos. Chem. Phys.*, *7*, 3385–3398, doi:10.5194/acp-7-3385-2007.

George, M., et al. (2009), Carbon monoxide distributions from the IASI/METOP mission: Evaluation with other space-borne remote sensors, *Atmos. Chem. Phys.*, *9*, 8317–8330, doi:10.5194/acp-9-8317-2009.

Gerbig, C., S. Schmitgen, D. Kley, A. Volz-Thomas, K. Dewey, and D. Haaks (1999), An improved fast-response vacuum-UV resonance fluorescence CO instrument, *J. Geophys. Res.*, *104*(D1), 1699–1704, doi:10.1029/1998JD100031.

Granier, C., J. F. Mueller, G. Petron, and G. Brasseur (1999), A three-dimensional study of the global CO budget, *Chemosphere Global Change Sci.*, *1*, 255–261, doi:10.1016/S1465-9972(99)00007-0.

Grell, G. A., S. E. Peckham, R. Schmitz, S. A. McKeen, G. Frost, W. C. Skamarock, and B. Eder (2005), Fully coupled online chemistry within the WRF model, *Atmos. Environ.*, *39*, 6957–6975, doi:10.1016/j.atmosenv.2005.04.027.

Guenther, A., T. Karl, P. Harley, C. Wiedinmyer, P. I. Palmer, and C. Geron (2006), Estimates of global terrestrial isoprene emissions using MEGAN (Model of Emissions of Gases and Aerosols from Nature), *Atmos. Chem. Phys.*, *6*, 3181–3210, doi:10.5194/acp-6-3181-2006.

Hansen, D. A., E. S. Edgerton, B. E. Hartsell, J. J. Jansen, N. Kandasamy, G. M. Hidy, and C. L. Blanchard (2003), The southeastern aerosol research and characterization study: Part 1 - Overview, *J. Air Waste Manage. Assoc.*, *53*, 1460–1471.

Herron-Thorpe, F. L., B. K. Lamb, G. H. Mount, and J. K. Vaughan (2010), Evaluation of a regional air quality forecast model for tropospheric NO_2 columns using the OMI/Aura satellite tropospheric NO_2 product, *Atmos. Chem. Phys.*, *10*, 8839–8854, doi:10.5194/acp-10-8839-2010.

Holloway, T., H. Levy II, and P. Kasibhatla (2000), Global distribution of carbon monoxide, *J. Geophys. Res.*, *105*, 12,123–12,147, doi:10.1029/1999JD901173.

Hu, X.-M., J. W. Nielsen-Gammon, and F. Zhang (2010), Evaluation of three planetary boundary layer schemes in the WRF model, *J. Appl. Meteorol. Climatol.*, *49*, 1831–1844, doi:10.1175/2010JAMC2432.1.

Huang, M., et al. (2010), Impacts of transported background ozone on California air quality during the ARCTAS-CARB period: A multi-scale modeling study, *Atmos. Chem. Phys.*, *10*, 6947–6968, doi:10.5194/acp-10-6947-2010.

Hudman, R. C., L. T. Murray, D. J. Jacob, D. B. Millet, S. Turquety, S. Wu, D. R. Blake, A. H. Goldstein, J. Holloway, and G. W. Sachse (2008), Biogenic versus anthropogenic sources of CO in the United States, *Geophys. Res. Lett.*, *35*, L04801, doi:10.1029/2007GL032393.

Jacob, D. J., J. H. Crawford, M. M. Kleb, V. S. Connors, R. J. Bendura, J. L. Raper, G. W. Sachse, J. C. Gille, L. Emmons, and C. L. Heald (2003), Transport and Chemical Evolution over the Pacific (TRACE-P) aircraft mission: Design, execution, and first results, *J. Geophys. Res.*, *108*(D20), 9000, doi:10.1029/2002JD003276.

Jacob, D. J., et al. (2010), The Arctic Research of the Composition of the Troposphere from Aircraft and Satellites (ARCTAS) mission: Design, execution, and first results, *Atmos. Chem. Phys.*, *10*, 5191–5212, doi:10.5194/acp-10-5191-2010.

Jaffe, D., I. Bertschi, L. Jaegle, P. Novelli, J. S. Reid, H. Tanimoto, R. Vingarzan, and D. L. Westphal (2004), Long-range transport of Siberian biomass emissions and impact on surface ozone in western North America, *Geophys. Res. Lett.*, *31*, L16106, doi:10.1029/2004GL020093.

Janjic, Z. I. (1996), The surface layer in the NCEP Eta Model, paper presented at Eleventh Conference on Numerical Weather Prediction, Am. Meteorol. Soc., Norfolk, Va., 19–23 Aug.

Janjic, Z. I. (2002), Nonsingular implementation of the Mellor-Yamada level 2.5 scheme in the NCEP Meso model, *Off. Note 437*, 61 pp., Natl. Cent. for Environ. Predict., Camp Springs, Md.

Kopacz, M., et al. (2010), Global estimates of CO sources with high resolution by adjoint inversion of multiple satellite datasets (MOPITT, AIRS, SCIAMACHY, TES), *Atmos. Chem. Phys.*, *10*, 855–876, doi:10.5194/acp-10-855-2010.

Lamarque, J.-F., et al. (2003), Identification of CO plumes from MOPITT data: Application to the August 2000 Idaho-Montana forest fires, *Geophys. Res. Lett.*, *30*(13), 1688, doi:10.1029/2003GL017503.

Logan, J. A., M. J. Prather, S. C. Wofsy, and M. B. McElroy (1981), Tropospheric chemistry: A global perspective, *J. Geophys. Res.*, *86*, 7210–7254, doi:10.1029/JC086iC08p07210.

Luo, M., et al. (2007), Comparison of carbon monoxide measurements by TES and MOPITT: The influence of a priori data and instrument characteristics on nadir atmospheric species retrievals, *J. Geophys. Res.*, *112*, D09303, doi:10.1029/2006JD007663.

Madronich, S. (1987), Photodissociation in the atmosphere: 1. Actinic flux and the effects of ground reflections and clouds, *J. Geophys. Res.*, *92*, 9740–9752, doi:10.1029/JD092iD08p09740.

Marenco, A., et al. (1998), Measurement of ozone and water vapor by AIRBUS in-service aircraft: The MOZAIC airborne program, An overview, *J. Geophys. Res.*, *103*, 25,631–25,642.

McMillan, W. W., et al. (2008), AIRS views transport from 12 to 22 July 2004 Alaskan/Canadian fires: Correlation of AIRS CO and MODIS AOD with forward trajectories and comparison of AIRS CO retrievals with DC-8 in situ measurements during INTEX-A/ICARTT, *J. Geophys. Res.*, *113*, D20301, doi:10.1029/2007JD009711.

McMillan, W. W., et al. (2010), An observational and modeling strategy to investigate the impact of remote sources on local air quality: A Houston, Texas, case study from the Second Texas Air Quality Study (TexAQS II), *J. Geophys. Res.*, *115*, D01301, doi:10.1029/2009JD011973.

Mellor, G. L., and T. Yamada (1982), Development of a turbulence closure model for geophysical fluid problems, *Rev. Geophys.*, *20*, 851–875, doi:10.1029/RG020i004p00851.

Miller, S. M., et al. (2008), Sources of carbon monoxide and formaldehyde in North America determined from high-resolution atmospheric data, *Atmos. Chem. Phys.*, *8*, 7673–7696, doi:10.5194/acp-8-7673-2008.

Mlawer, E. J., S. J. Taubman, P. D. Brown, M. J. Iacono, and S. A. Clough (1997), Radiative transfer for inhomogeneous atmosphere: RRTM, a validated correlated-k model for longwave, *J. Geophys. Res.*, *102*, 16,663–16,682, doi:10.1029/97JD00237.

Nedelec, P., J.-P. Cammas, V. Thouret, G. Athier, J.-M. Cousin, C. Legrand, C. Abonnel, F. Lecoeur, G. Cayez, and C. Marizy (2003), An improved infrared carbon monoxide analyser for routine measurements aboard commercial Airbus aircraft: Technical validation and first scientific results of the MOZAIC III programme, *Atmos. Chem. Phys.*, *3*, 1551–1564, doi:10.5194/acp-3-1551-2003.

Pan, L. L., et al. (2010), The Stratosphere-Troposphere Analyses of Regional Transport 2008 (START08) experiment, *Bull. Am. Meteorol. Soc.*, *91*, 327–342, doi:10.1175/2009BAMS2865.1.

Peng, L., Z. Chunsheng, L. Yunping, Z. Xiangdong, T. Xuexi, and C. Lo-Yin (2007), Analysis of carbon monoxide budget in North China, *Chemosphere*, *66*, 1383–1389, doi:10.1016/j.chemosphere.2006.09.055.

Pfister, G. G., G. Petron, L. K. Emmons, J. C. Gille, D. P. Edwards, J.-F. Lamarque, J.-L. Attie, C. Granier, and P. C. Novelli (2004), Evaluation of CO simulations and the analysis of the CO budget for Europe, *J. Geophys. Res.*, *109*, D19304, doi:10.1029/2004JD004691.

Pfister, G. G., L. K. Emmons, D. P. Edwards, A. Arellano, G. Sachse, and T. Campos (2010), Variability of springtime transpacific pollution transport during 2000–2006: The INTEX-B mission in the context of previous years, *Atmos. Chem. Phys.*, *10*, 1345–1359, doi:10.5194/acp-10-1345-2010.

Pfister, G. G., et al. (2011a), Characterizing summertime chemical boundary conditions for airmasses entering the U.S. West Coast, *Atmos. Chem. Phys.*, *11*, 1769–1790, doi:10.5194/acp-11-1769-2011.

Pfister, G. G., J. Avise, C. Wiedinmyer, D. P. Edwards, L. K. Emmons, G. D. Diskin, J. Podolske, and A. Wisthaler (2011b), CO source contribution analysis for California during ARCTAS-CARB, *Atmos. Chem. Phys. Discuss.*, *11*, 3627–3661, doi:10.5194/acpd-11-3627-2011.

Piters, A. J. M., K. Bramstedt, J.-C. Lambert, and B. Kirchhoff (2006), Overview of SCIAMACHY validation: 2002–2004, *Atmos. Chem. Phys.*, *6*, 127–148, doi:10.5194/acp-6-127-2006.

Rinsland, C. P., et al. (2006), Nadir measurements of carbon monoxide (CO) distributions by the tropospheric emission spectrometer instrument onboard the Aura spacecraft: Overview of analysis approach and examples of initial results, *Geophys. Res. Lett.*, *33*, L22806, doi:10.1029/2006GL027000.

Rodgers, C. D., and B. J. Connor (2003), Intercomparison of remote sounding instruments, *J. Geophys. Res.*, *108*(D3), 4116, doi:10.1029/2002JD002299.

Seinfeld, J. H., and S. N. Pandis (2006), *Atmospheric Chemistry and Physics: From Air Pollution to Climate Change*, John Wiley, Hoboken, N. J.

Skamarock, W. C., J. B. Klemp, J. Dudhia, D. O. Gill, D. M. Barker, M. Duda, X.-Y. Huang, W. Wang, and J. G. Powers (2008), A description of the Advanced Research WRF version 3, *NCAR Tech. Note NCAR/TN–475 + STR*, 125 pp., Natl. Cent. for Atmos. Res., Boulder, Colo.

Smirnova, T. G., J. M. Brown, and S. G. Benjamin (1997), Performance of different soil model configurations in simulating ground surface temperature and surface fluxes, *Mon. Weather Rev.*, *125*, 1870–1884, doi:10.1175/1520-0493(1997)125<1870:PODSMC>2.0.CO;2.

Smirnova, T. G., J. M. Brown, S. G. Benjamin, and D. Kim (2000), Parameterization of cold-season processes in the MAPS land-surface scheme, *J. Geophys. Res.*, *105*, 4077–4086, doi:10.1029/1999JD901047.

Thompson, A. M., and R. J. Cicerone (1986), Possible perturbations of atmospheric CO, CH4 and OH, *J. Geophys. Res.*, *91*, 10,853–10,864, doi:10.1029/JD091iD10p10853.

Turquety, S., et al. (2008), CO emission and export from Asia: An analysis combining complementary satellite measurements (MOPITT, SCIAMACHY and ACE-FTS) with global modeling, *Atmos. Chem. Phys.*, *8*, 5187–5204, doi:10.5194/acp-8-5187-2008.

U. S. Environmental Protection Agency (1991), Air quality criteria for carbon monoxide, *Rep. EPA/600/8–90/045F*, Off. of Health and Environ. Assess., Research Triangle Park, N. C.

U. S. Environmental Protection Agency (2000), Air quality criteria for carbon monoxide, *Rep. EPA/600/P-99/001F*, Off. of Health and Environ. Assess., Research Triangle Park, N. C.

Vogel, B., et al. (2011), Transport pathways and signatures of mixing in the extratropical tropopause region derived from Lagrangian model simulations, *J. Geophys. Res.*, *116*, D05306, doi:10.1029/2010JD014876.

Warner, J. X., M. McCourt Comer, C. Barnet, W. W. McMillan, W. Wolf, E. Maddy, and G. Sachse (2007), A comparison of satellite tropospheric carbon monoxide measurements from AIRS and MOPITT during INTEXNA, *J. Geophys. Res.*, *112*, D12S17, doi:10.1029/2006JD007925.

Wesely, M. L. (1989), Parameterization of surface resistance to gaseous dry deposition in regional-scale numerical models, *Atmos. Environ.*, *23*, 1293–1304, doi:10.1016/0004-6981(89)90153-4.

Wiedinmyer, C., B. Quayle, C. Geron, A. Belote, D. McKenzie, X. Zhang, S. O'Neill, and K. K. Wynne (2006), Estimating emissions from fires in North America for air quality monitoring, *Atmos. Environ.*, *40*, 3419–3432, doi:10.1016/j.atmosenv.2006.02.010.

Wiedinmyer, C., S. K. Akagi, R. J. Yokelson, L. K. Emmons, J. A. Al-Saadi, J. J. Orlando, and A. J. Soja (2010), The Fire Inventory from NCAR (FINN): A high resolution global model to estimate the emissions from open burning, *Geosci. Model Dev. Discuss.*, *3*, 2439–2476, doi:10.5194/gmdd-3-2439-2010.

Wigley, T. M. L., S. J. Smith, and M. J. Prather (2002), Radiative forcing due to reactive gas emissions, *J. Clim.*, *15*(18), 2690–2696, doi:10.1175/1520-0442(2002)015<2690:RFDTRG>2.0.CO;2.

Worden, H. M., M. N. Deeter, D. P. Edwards, J. C. Gille, J. R. Drummond, and P. Nédélec (2010), Observations of near-surface carbon monoxide from space using MOPITT multispectral retrievals, *J. Geophys. Res.*, *115*, D18314, doi:10.1029/2010JD014242.

Zhang, L., et al. (2008), Transpacific transport of ozone pollution and the effect of recent Asian emission increases on air quality in North America: An integrated analysis using satellite, aircraft, ozonesonde, and surface observations, *Atmos. Chem. Phys.*, *8*, 6117–6136, doi:10.5194/acp-8-6117-2008.

Zyrichidou, I., et al. (2009), Satellite observations and model simulations of tropospheric NO_2 columns over south-eastern Europe, *Atmos. Chem. Phys.*, *9*, 6119–6134, doi:10.5194/acp-9-6119-2009.

A. Boynard, D. P. Edwards, and G. G. Pfister, Atmospheric Chemistry Division, National Center for Atmospheric Research, PO Box 3000, Boulder, CO 80307-3000, USA. (boynard@ucar.edu; edwards@ucar.edu; pfister@ucar.edu)